NET Final Report – Submitted April 4, 2012

Project: Riparian Vegetation Impacts on Water Quantity, Quality, and Stream Ecology

Principal Investigators: Durelle Scott, Erkan Istanbulluoglu, John Lenters, and Kyle Herrman

Reporting period: April 2008 – March 2012

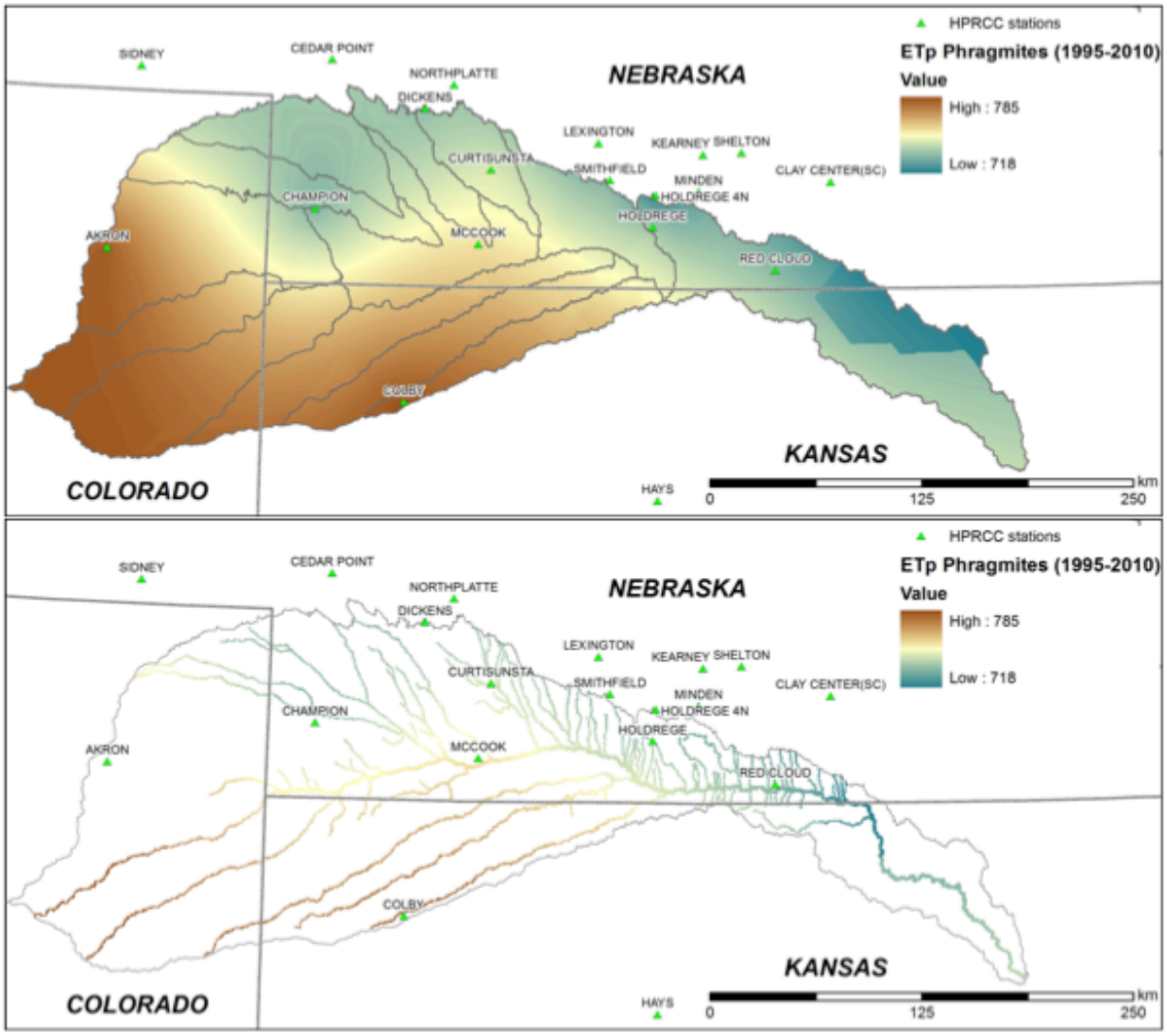

Table of Contents

Project Overview 2

1. First-order evapotranspiration (ET) estimates 3
2. Energy and water balance observations from a *P. australis*-dominated wetland 5
3. Observed impacts of *P. australis* removal on evapotranspiration 12
4. Carbon dynamics, biogeochemistry, and stream metabolism 17
   a. Carbon dynamics in the *P. australis* wetland 17
   b. Impact of *P. australis* on wetland biogeochemistry 19
   c. Effects on stream metabolism 21
5. Growth chamber measurements of plant physiology 24
6. Agro-IBIS model results 26
   a. Agro-IBIS simulations at the wetland field site 26
   b. Agro-IBIS regional simulations 27
7. List of publications 31
8. List of presentations 32

Project Overview

Riparian areas are critical zones on the landscape, representing the intersection between upland terrestrial ecosystems and water bodies. Active riparian areas within watersheds provide multiple ecological and human benefits. Both water and energy cycles within riparian areas are governed by complex non-linear interactions, as changes in one may result in changes in all others, often degrading water quantity and quality, fish populations, public health, and recreation. Species diversity and other riparian ecosystem services are largely maintained on the landscape by disturbance events, including fires, floods, and grazing. However, fire suppression and flood control via dams has decreased natural disturbance regimes in riparian areas, resulting in the invasion of non-native vegetation across the western United States including Nebraska.

Non-native species within Nebraska‘s riparian areas include Tamarisk (Salt Cedar), *Phragmites australis*, and Russian olive. Across Nebraska, multiple agencies (e.g. FWS, NRD’s) are involved in removing invasive species for two primary reasons: (1) providing habitat for wildlife (e.g. Central Platte River), and (2) reducing riparian water consumption (esp. in the Republican River basin). However, the overall water savings by invasive species removal and the impacts on aquatic ecosystems are largely uncertain.

The overall goal of this NET-funded project has been to develop a quantitative understanding of the role of riparian vegetation dynamics, including invasive species, on the interactions among hydrology, ecology, geomorphology, and chemistry of streams and riparian zones within the Republican and Platte River basins. Specific study objectives related to this goal include:

1. Producing a first-order estimate of riparian evapotranspiration (ET) for the Republican River basin
2. Estimating water consumption by *P. australis* through direct measurements of ET
3. Calculating potential water savings from invasive species removal along riparian corridors using direct observations and an ecosystem / land surface model (Agro-IBIS)
4. Assessing the impacts of riparian *P. australis* removal on stream water quality
5. Evaluating wetland nitrogen and carbon cycling by invasive and native vegetation
6. Measuring relevant *P. australis* physiological parameters for use in numerical modeling

This final report provides a summary of the accomplishments related to the above project objectives. For more detailed results of the study, the reader is referred to the project publications listed in section 7 of this report, as well as the numerous previous quarterly reports submitted to the NET over the course of the project.

1. First-order evapotranspiration (ET) estimates

We calculated "first-order estimates" of riparian ET in the Republican River basin using climate data from the High Plains Regional Climate Center (HPRCC). Radiation and temperature data from numerous locations within and surrounding the basin were used to calculate Priestley-Taylor estimates of "potential ET." This potential rate of maximum ET was then scaled down to "actual ET" using crop coefficients for *P. australis* that were calculated from our 2009 energy balance analysis at the wetland field site (Lenters et al., 2011; Cutrell 2010). The resulting ET values were then overlaid on GIS maps of the Republican River and its main tributaries (Figure 1) and integrated over a hypothetical riparian buffer zone (of varying width). Estimates of consumptive water use from *P. australis* (as a function of riparian area) are provided in Figure 2. A hypothetical maximum riparian area of 5750 km^2 was estimated by assuming a buffer width of 1 km for the main stem of the Republican River (with tributaries assumed to be half as wide).

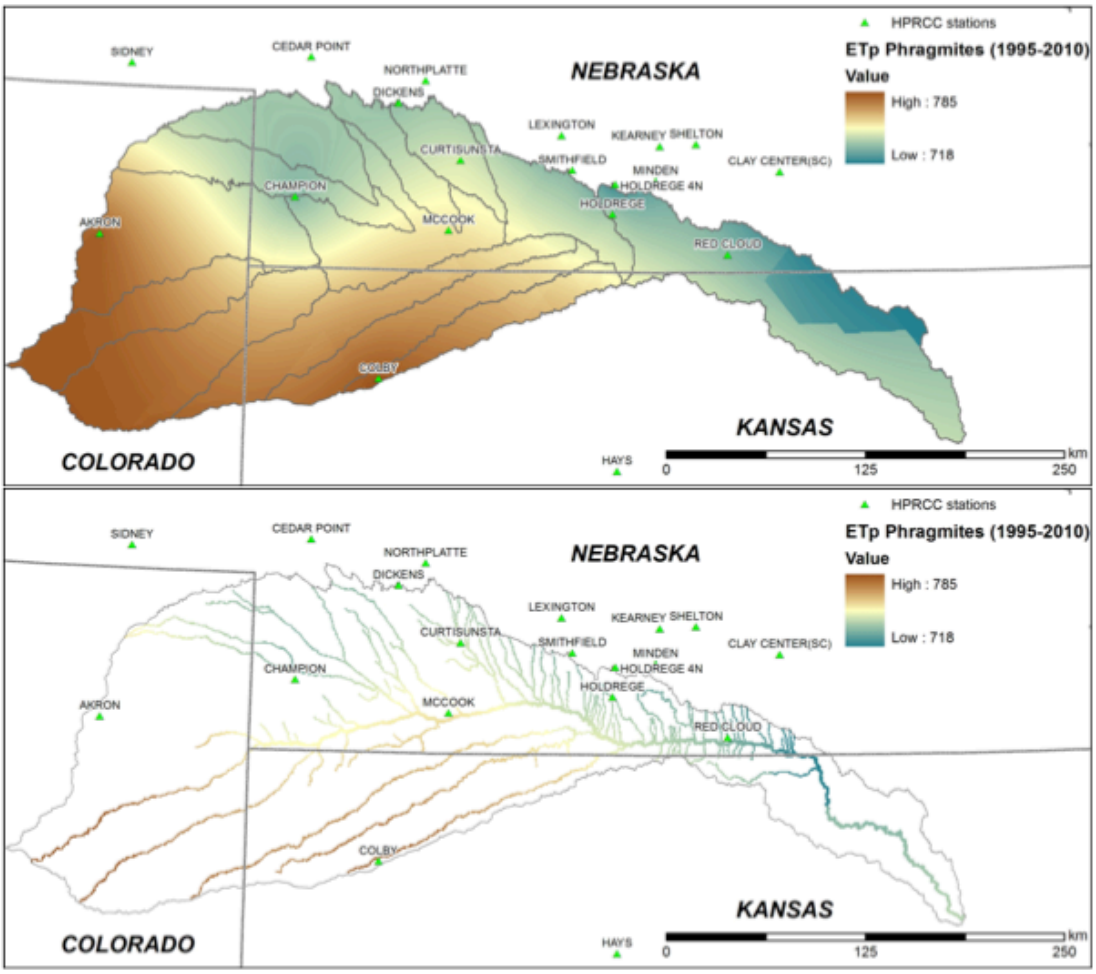

Figure 1. First-order estimates of mean annual potential ET for *P. australis* over a) the entire Republican River basin and b) just the riparian zone. Potential ET (in mm) was calculated via the Priestley-Taylor method and then (later) "scaled down" to actual ET using crop coefficients (calculated from measured ET at the wetland field site near Arapahoe).

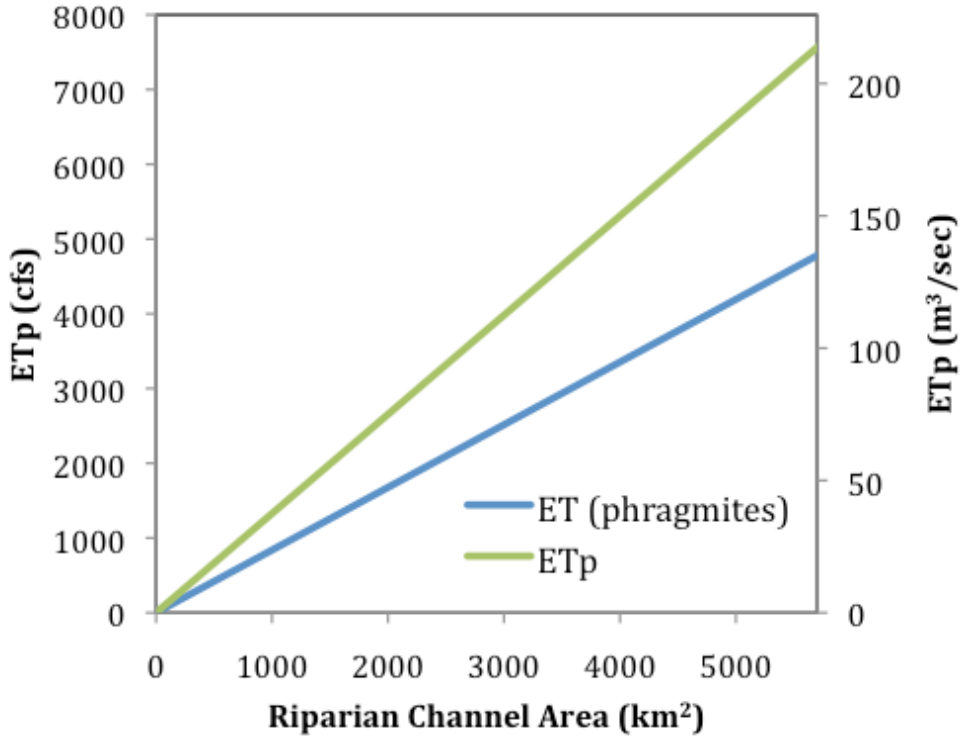

Figure 2. First-order estimates of mean annual potential ET (ET_P) and actual ET from a hypothetically 100%-infested *P. australis* riparian zone within the Republican River basin. The total, integrated ET is shown as a function of riparian zone area, in which the maximum channel area of 5750 km^2 corresponds to a main-stem channel width of 1 km (0.5 km for tributaries). The integrated ET rates are shown in units of both cfs and m^3/s.

The results of the first-order ET estimate show that mean annual potential ET rates vary spatially by only +/- 5% (Figure 1) – from roughly 785 mm in the western Republican River basin to about 720 mm in the eastern portions of the basin. Integrated over the entire hypothetical riparian zone (and scaled down to "actual" ET rates), we estimate that *P. australis* within a 1-km main-stem buffer would use water at an annual mean rate of almost 5000 cfs (Figure 2). This, of course, assumes 100% infestation by invasive *P. australis*, as well as a relatively wide main-stem riparian zone of 1 km (0.5 km in tributaries). The effect of reduced riparian areas (i.e., narrower buffers and/or reduced infestation) can be assessed through the use of Figure 2. Thus, for example, a 20% infestation rate and main-stem width of 0.25 km would result in a 20-fold reduction in the estimated basin-wide water use by *P. australis* within the riparian zone (i.e., roughly 200-250 cfs).

It is important to note that the ET values shown in Figure 2 do not represent the amount of water **savings** that would result from the **removal** of *P. australis*. Rather, they represent estimates of the **total water use** by *P. australis* and, therefore, are only an upper bound on the potential water savings that could be achieved by vegetation removal. Actual water savings would, of course, depend on the type of land cover that replaced the *P. australis* (and its associated ET rate).

2. Energy and water balance observations from a *P. australis*-dominated wetland

In this section, estimation of the ET rate from *P. australis* during the 2009 growing season is provided, as well as the diurnal, daily, and seasonal variability in the surface energy and water balance. Although the wetland was sprayed with herbicide in late July of 2009 (to assess the impact of vegetation removal), a clear response to this spraying was not evident until the 2010 growing season. Therefore, the results of the herbicide treatment are not presented in this section but a comparative analysis of the 2009 and 2010 seasons will instead be discussed in the next section. More detailed information can be found in Lenters et al. (2011) related to the 2009 growing season energy and water balance.

Daily precipitation, water level, air temperature, relative humidity, surface water temperature, and wind speed (all measured at the wetland study site) are shown in Figure 3 for the 2009 growing season. Water levels increased from the beginning of the growing season until late June, after which they steadily decreased until September and then leveled off through the end of the growing season. Daily air temperatures were much more variable than the wetland water temperatures, but they generally oscillated about similar mean values through early June. For the remainder of the year, however, the air temperature was notably warmer than the surface water temperature, particularly from mid-June to mid-August (Figure 3). This is primarily due to the strong shading (and insulating) effect of the tall *P. australis* vegetation on the underlying water column, as well as the high latent heat flux that occurs from the canopy. Groundwater and soil heat flux also exert a cooling influence on the wetland water temperatures during the majority of the growing season.

Daily mean wind speeds at the wetland site were generally strongest during April, May, and late September (Figure 3), in association with extratropical storms and frontal activity. Prevailing wind directions in the spring tended to be out of the northwest or southeast (Cutrell, 2010), while winds during June–September were predominantly easterly and much weaker (with occasional northwesterly winds that were stronger, but less common). Even though the anemometer at the wetland station is mounted at a height of over 6 m above the soil/water interface (i.e., ~2 m above the maximum canopy height), it is noteworthy that the daily mean wind speeds are generally quite weak (usually less than 1 m s^{-1} during June–September). Daily mean wind speeds at a nearby High Plains Regional Climate Center (HPRCC) Automated Weather Data Network (AWDN) station in Holdrege, Nebraska, for example, are typically around 3–4 m s^{-1}. We attribute the reduction in wind speeds at our wetland site to the "wind shading" effect of the sparse cottonwood trees that surround the wetland, as well as the added surface resistance that occurs in conjunction with the growth of the tall *P. australis* vegetation. Weaker daytime surface mixing, in association with strong evaporative cooling in the wetland and surrounding agricultural fields, may also be responsible for some of the reduced wind speeds.

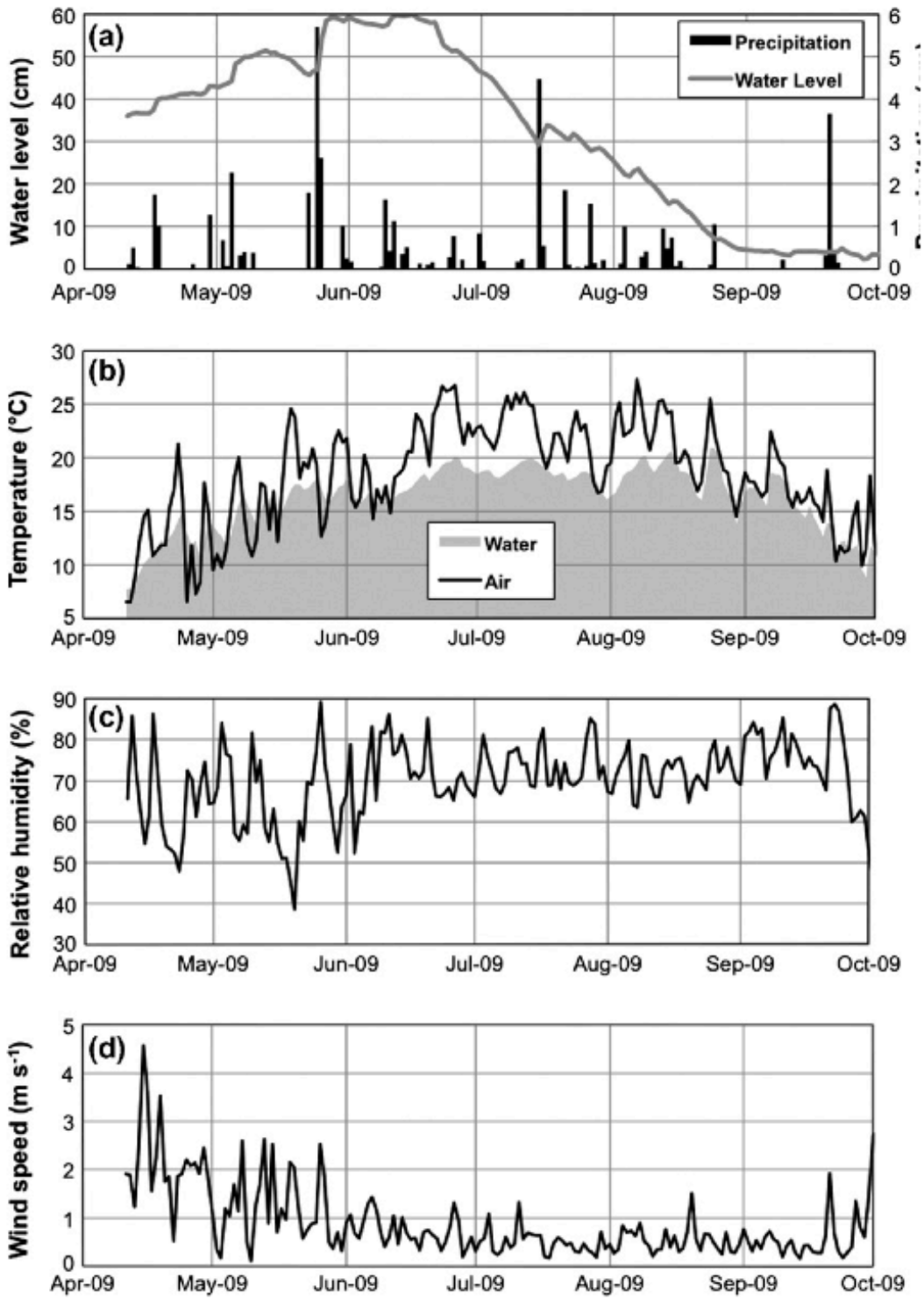

Figure 3. Daily mean (a) precipitation and water level, (b) air temperature and surface water temperature, (c) relative humidity, and d) wind speed, as measured at the *P. australis* meteorological station during the 2009 growing season.

Surface Radiation Balance

Figure 4 shows 5-day running mean values of incoming shortwave radiation (SW_{in}), incoming longwave radiation (LW_{in}), net longwave radiation ($LW_{net} = LW_{in} - LW_{out}$), and net all-wave radiation ($R_n = SW_{in} - SW_{out} + LW_{net}$). SW_{in} shows the largest variation, ranging from a 5-day minimum of 103 W m^{-2} on September 23 to a 5-day maximum of 353 W m^{-2} on May 30. These variations in solar radiation are related to seasonal changes in sun angle and daylength, as well as changes in cloud cover (Figure 5) that occurred in association with extratropical cyclones and fronts (and/or summertime convection). Generally, the month of June would be expected to receive more incoming solar radiation than May, due to the higher sun angle during that time. But significant cloud cover in June of 2009 resulted in lower SW_{in} than during May, July, and even August. As a result, changes in R_n are largely associated with variations in sun angle and cloud cover, with the season-mean R_n being ~160 W m^{-2}.

The 5-day running mean albedo (5-day SW_{out} divided by 5-day SW_{in}) shows moderate seasonal variation over the course of the growing season in the *P. australis* portion of the wetland (Figure 5). Daily albedo values ranged from a minimum of 0.16 on April 17 to a maximum of 0.24 on June 8. We attribute some of this seasonal increase in albedo to the greening up and "leafing out" of the *P. australis*, which would obscure some of the exposed (and darker) water surface beneath the plant canopy. As illustrated in Figure 5, the *P. australis* albedo values subsequently declined later in the season (beginning in late July), presumably in response to reductions in LAI in association with senescence (and possibly herbicide spraying, which was applied in late July).

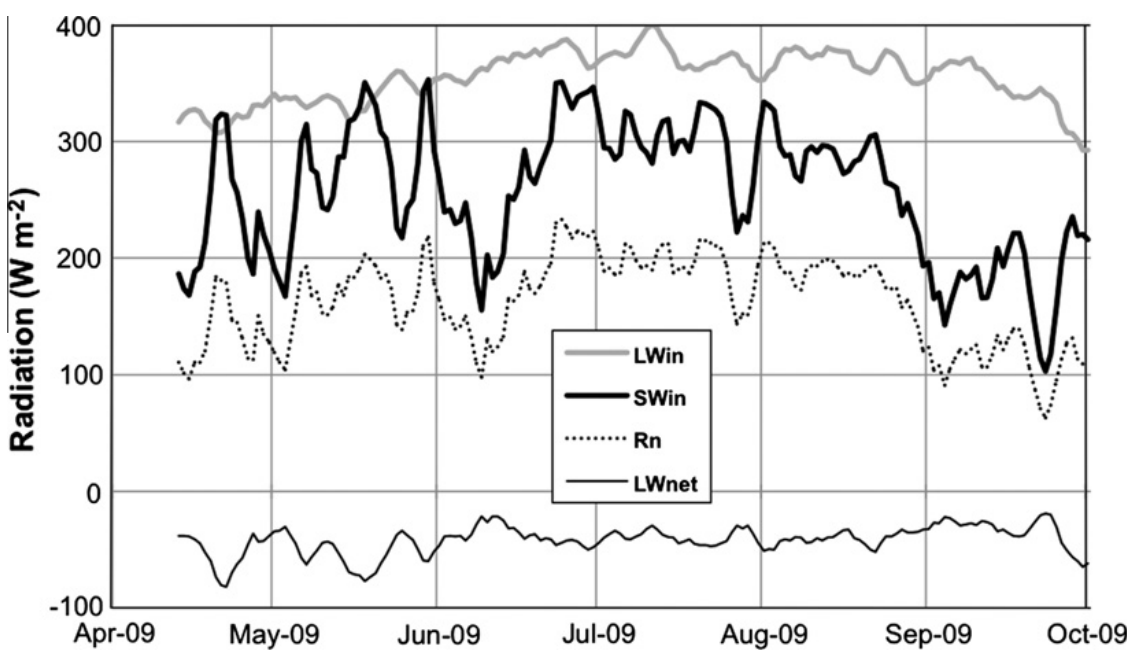

Figure 4. 5-day running mean radiation balance showing the incoming shortwave radiation (SW_{in}), incoming longwave (LW_{in}), net longwave (LW_{net}), and total net radiation (R_n) during the 2009 growing season. Measurements were made at the *P. australis* meteorological station.

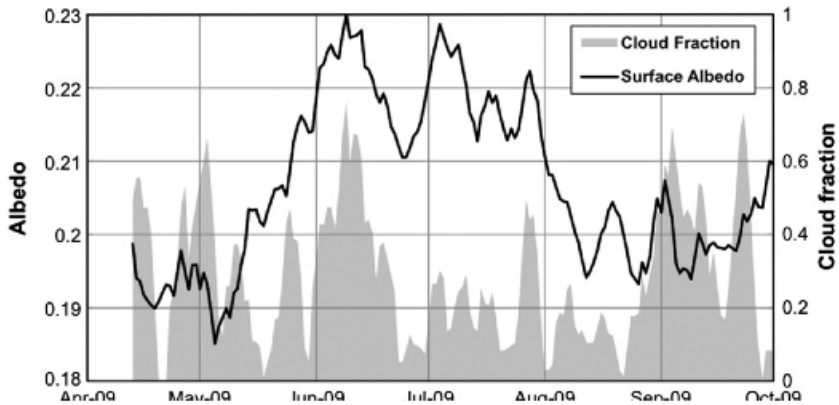

Figure 5. Cloud fraction and shortwave surface albedo measured at the *P. australis* meteorological station during the 2009 season. Values are based on 5-day running mean measurements of incoming and reflected solar radiation, as well as theoretical clear sky values of incoming solar radiation for the given latitude and time period.

Heat Storage Rate

The 5-day running mean heat storage rate of the wetland is shown in Figure 6, broken down into three components: (1) upper soil, (2) deep soil, and (3) total heat storage rate. Heat storage in the water column (not shown explicitly in Figure 6) makes up the majority of the total heat storage term, except for times late in the season when water levels were low (Figure 3a). In general, the rate of heat storage in the upper and deep soil layers is somewhat lagged and has considerably less variability than that of the water (and, therefore, the total). Canopy heat storage (air + vegetation; not shown) is essentially negligible on daily timescales, with a seasonal mean of ~0.02 W m^{-2} and a daily standard deviation (0.67 W m^{-2}) that is roughly 4% that of the total heat storage term (as compared to 6%, 22%, and 96% for the deep soil, upper soil, and water column, respectively). Overall, the daily heat storage rate in the water column ranged from a minimum of ~67.0 W m^{-2} in late April (out of a total heat storage rate of ~61.3 W m^{-2}) to a maximum of +51.7 W m^{-2} in early May (out of a total of +55.9 W m^{-2}).

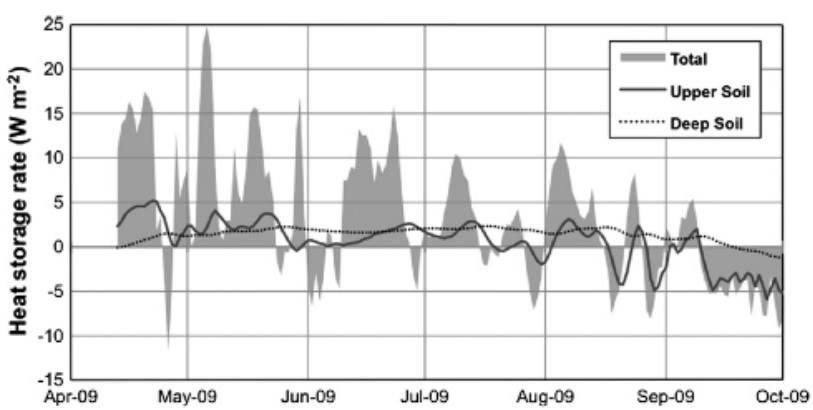

Figure 6. 5-day running mean heat storage rate as measured in the *P. australis* portion of the wetland during the 2009 season. Separate heat storage rates for the "upper" and "deep" soil layers are shown as solid and dotted lines, respectively. The total heat storage rate (shaded gray) includes heat stored in the two soil layers, as well as the water column and vegetation/air canopy.

Sensible heat flux

Results of the 5-day running mean energy balance (Figure 7) reveal significant seasonal variations in the magnitude of the sensible heat flux, with highest 5-day mean values occurring during April and May (~50–150 W m^{-2}), prior to the full development of the *P. australis* vegetation. The high sensible heat flux is indicative of the high wind speeds and dry vegetation at this time of year and comprises a significant fraction of the available energy (net radiation minus heat storage rate; see Figure 8). Bowen ratios often exceed 1.0 prior to early May (Figure 8 and Table 1). By early June, sensible heat flux values declined significantly to ~15–20 W m^{-2} in association with corresponding increases in latent heat flux (Figures 7 and 8) and decreases in wind speed (Figure 3d). The sensible heat flux stayed low throughout most of the remaining growing season, aside from a slight increase in late September, presumably in response to higher wind speeds and vegetation senescence.

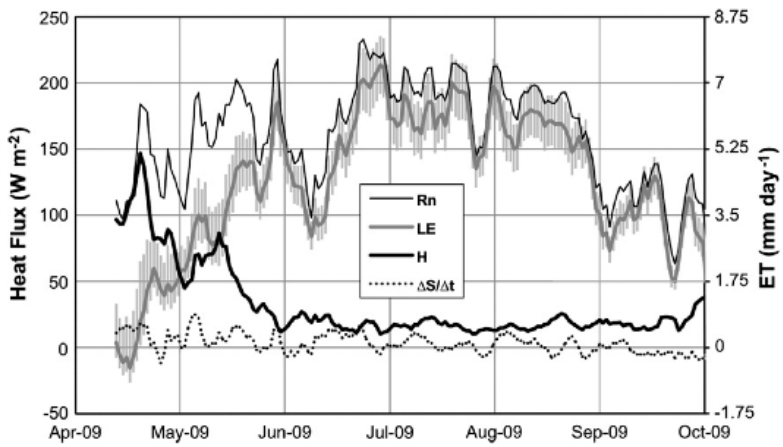

Figure 7. 5-day running mean energy balance components, including net radiation (R_n), total rate of change in heat storage *(ΔS/Δt)*, sensible heat flux (*H*), and latent heat flux (*LE*; also shown as ET in mm day^{-1} on the right hand side). Gray error bars represent the potential error in LE that could result from (cumulative) maximum uncertainties in other energy balance terms.

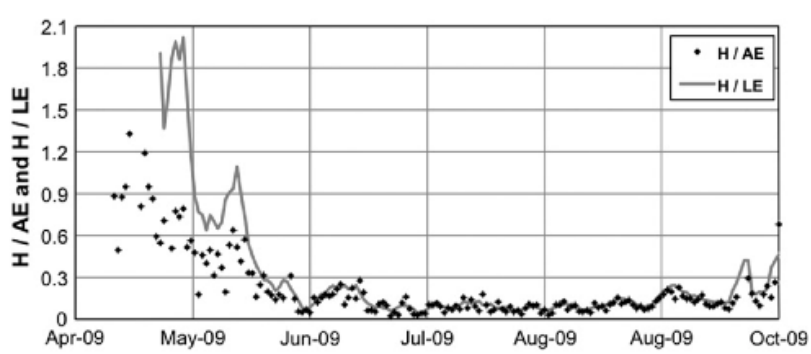

Figure 8. Ratio of the daily mean sensible heat flux (*H*) to the daily available energy (*LE*) during the 2009 growing season (solid black diamonds). Also shown is the 5-day Bowen ratio (gray line), in which *B* = (5-day *H*)/(5-day *LE*). Note that the Bowen ratio prior to April 23 is not plotted (due to *LE* values near zero, which leads to large fluctuations in *B*).

Table 1. Monthly mean energy balance components and Bowen ratio ($B = H/LE$) for the *P. australis* portion of the wetland from April 11 to October 3, 2009. (October is included in September's calculations, and April averages represent only a partial month.) Also shown are the standard deviations within each month (±), based on the daily mean values. All units are in W m^{-2} (except for B, which is unitless). The first Bowen ratio value represents the ratio of the monthly mean H and monthly mean LE, while parenthetical values for B show the mean daily Bowen ratio and its standard deviation within that month.

	SW_{in}	R_n	$\Delta S/\Delta t$	H	LE	B
April	227 ± 103	132 ± 63	10 ± 22	99 ± 47	23 ± 35	4.3 (3.33 ± 6.29)
May	275 ± 98	167 ± 60	8 ± 20	49 ± 28	110 ± 48	0.45 (0.58 ± 0.44)
June	264 ± 100	169 ± 66	4 ± 18	18 ± 10	147 ± 56	0.12 (0.15 ± 0.10)
July	296 ± 68	192 ± 45	2 ± 7	17 ± 6	174 ± 42	0.10 (0.10 ± 0.04)
August	280 ± 50	183 ± 31	2 ± 10	17 ± 6	164 ± 30	0.10 (0.11 ± 0.04)
September	185 ± 62	111 ± 38	−4 ± 9	22 ± 12	93 ± 37	0.24 (0.32 ± 0.40)

Latent heat flux

Latent heat flux values showed considerable seasonal variability in the *P. australis* wetland (Figure 7), with minimum values of roughly zero in mid-April to 5-day averages exceeding 200 W m^{-2} in late June (corresponding to a rate of water loss of over 7 mm day^{-1}). The latent heat flux then declined to around 100 W m^{-2} by the end of the season. On daily mean timescales, the minimum LE was ~35.6 W m^{-2} (~1.3 mm day^{-1}) on April 14, and the maximum was 233.0 W m^{-2} (8.2 mm day^{-1}) on June 29. (Although somewhat uncertain due to associated error bounds, condensation events early in the season are potentially related to the low water temperatures in the wetland in combination with occasional warm, humid air masses.) The maximum daily ET reported in this study is somewhat higher than previously measured *P. australis* ET values in different regions and under different conditions. On the other hand, a maximum daily ET rate of ~8.0 mm day^{-1} was found in an energy balance study of *P. australis* for a different vegetated river system in Nebraska (A. Irmak, personal communication, 8 August 2010), which is within 2–3% of the value found in the present study.

Water Balance

In this section, we relate changes in water level to other components of the water balance to provide additional corroboration of the calculated ET rates, as well as to examine the role of groundwater fluxes in the wetland water balance. We do not attempt to provide rigorous closure of the water balance, as groundwater and surface water fluxes were not directly measured. Rather, we simply compare daily water level measurements with timeseries of cumulative P - ET, and then interpret the level of agreement or disagreement between these two timeseries. The results are shown in Figure 9 (along with the cumulative precipitation), using the initial wetland water level (L_0) as the starting point for both timeseries. The evolution of the water level (L_t) and cumulative P - ET curves through time is similar, particularly on short timescales (e.g., individual precipitation events) and in terms of the overall trend from the beginning to end of the growing season (with both curves declining by a total of ~30 cm). This lends additional credence to the observed precipitation values and energy balance-derived ET rates.

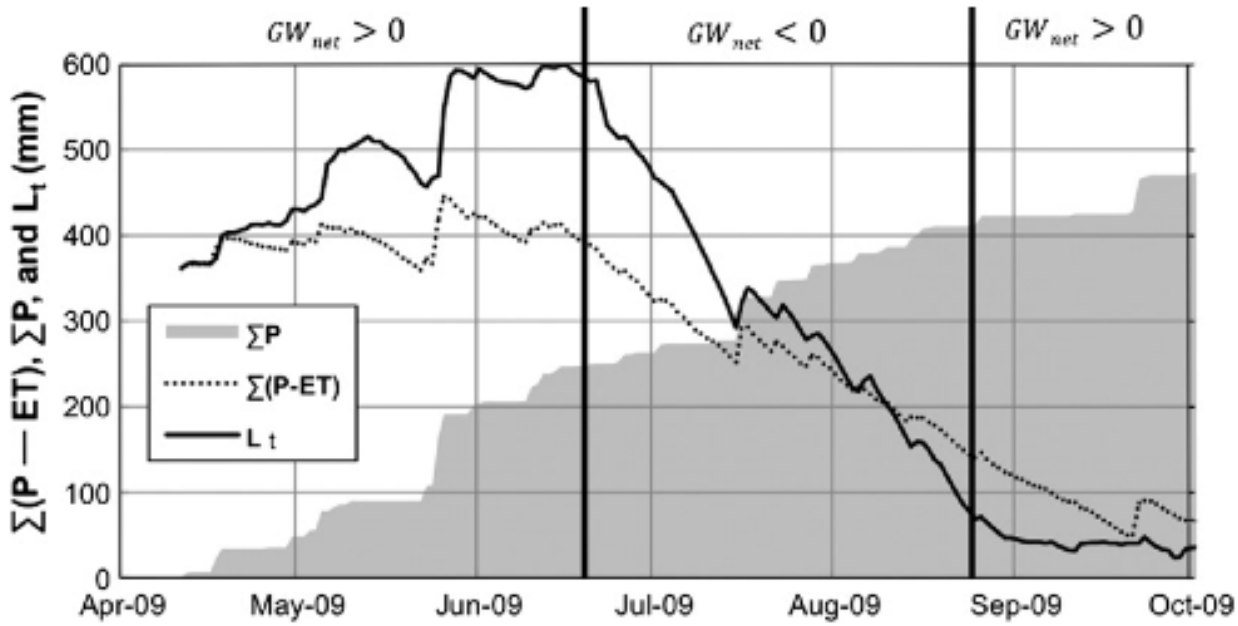

Figure 9. Daily cumulative precipitation (; shaded gray), wetland water level (L_t; solid line), and cumulative precipitation minus ET (**Figure 9**. Daily cumulative precipitation ($\sum P$; shaded gray), wetland water level (L_t; solid line), and cumulative precipitation minus ET ($\sum(P - ET)$; dotted line). ET is calculated from the energy balance, and the initial water level (L_0) is used as the starting point for $\sum(P - ET)$. Thick, vertical lines represent transitions between periods of net groundwater influx ($GW_{net} > 0$) and outflux ($GW_{net} < 0$). Surface inflow/outflow is assumed to be negligible relative to other water balance components.

On the other hand, there are also three broad periods of disagreement between the slopes of the two curves (delineated by the two vertical bars in Figure 9). In the first instance (roughly mid-April through mid-June), the wetland water level generally increased at a faster rate than the cumulative *P - ET* curve. This indicates an additional flux of water into the wetland that was not explicitly measured or accounted for. As noted earlier, we interpret this as a net influx of groundwater (i.e., discharge), since surface flow into or out of the wetland is minimal. By late June, this pattern of net groundwater discharge ($GW_{net} > 0$) changes to recharge ($GW_{net} < 0$), as reflected in the greater drop in water level relative to the cumulative *P - ET* curve (Figure 9). This period of recharge continues through late August and may be partly associated with groundwater withdrawals in the nearby agricultural fields, since this is the high water-demand period of the growing season. Finally, by the end of August, the scenario switches back to one of groundwater discharge, and the two water budget terms settle to a similar end-of-season value. This latter observation suggests that the net flux of groundwater into or out of the wetland, when averaged over the entire growing season, is relatively small.

3. Observed impacts of *P. australis* removal on evapotranspiration

Energy balance calculations were conducted using data from the 2010 growing season (i.e., when the *P. australis* vegetation was dead – having been sprayed with herbicide the previous year). Due to the lack of live vegetation at the Bowen ratio station in the *P. australis* section of the wetland during 2010 (i.e., much lower leaf area index [LAI] than in 2009), there is a greater amount of water exposed to incoming solar radiation. And since water is a darker surface than vegetation (reflecting about 1/3 as much sunlight), this led to a decrease in the overall albedo (i.e., reflectivity) of the wetland in 2010 (Figure 10). This was a somewhat surprising result, since the dead, brown vegetation appears "brighter" to the naked eye than live, green vegetation. But this effect is apparently counteracted by the lower LAI and greater exposure to darker water underneath. The difference in albedo began to be noticeable around late April (Figure 10), which is approximately the same time that the vegetation began to "green up" in 2009.

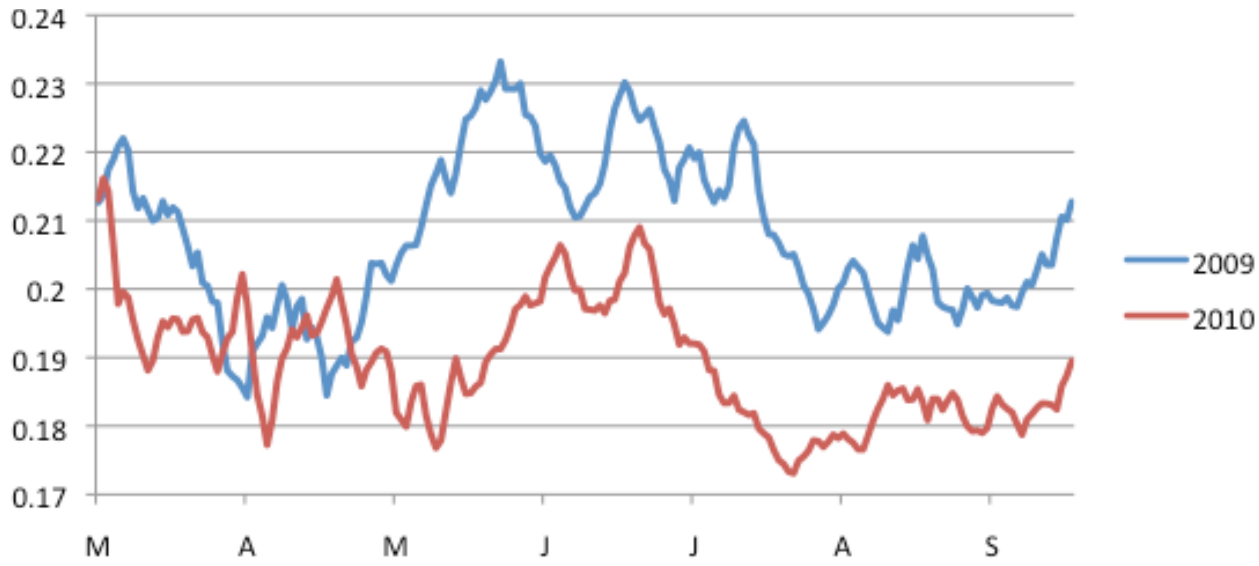

Figure 10. Five-day running mean surface albedo (ratio of reflected to incoming solar radiation) for the *P. australis* section of the wetland during the past two growing seasons. Note the overall "darker" surface during 2010 (presumably due to lower LAI and greater absorption of solar radiation by water).

In addition to albedo, there was also a noticeable deviation in wetland surface temperature during 2010 between the *P. australis* and native portions of the wetland, with the (dead) *P. australis* section being distinctly warmer than the native (Figure 11). This deviation was not present in 2009, suggesting that the difference in 2010 is due to reduced evaporative cooling from the *P. australis* (i.e., lower evapotranspiration), as well as greater absorption of solar radiation (lower albedo). Similar to the albedo, this difference is first noticeable in early May, when the vegetation typically greens up.

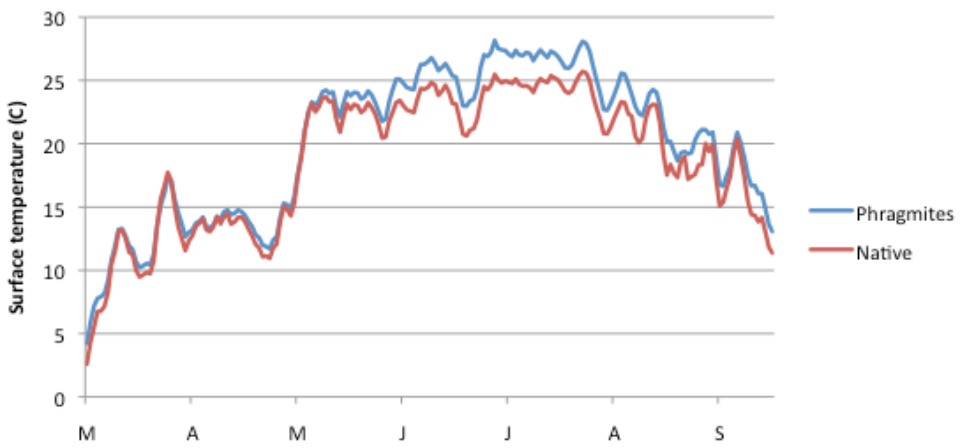

Figure 11. Five-day running mean surface temperature (measured by infrared radiometers) for the *P. australis* (blue) and native (red) portions of the wetland. Note the deviation in temperatures beginning in early May (which did not show up at all in the 2009 data).

Estimates of LAS-derived sensible heat flux over the *P. australis* vegetation are shown in Figure 12. It is clear that the herbicide spraying of the *P. australis* had a dramatic effect on the energy balance of the wetland. As would be expected, the difference shows up most significantly during the main part of the growing season, due to the greening-up of vegetation that occurred in 2009 (but not 2010). The sensible heat flux during the 2010 growing season is roughly three times that of 2010, indicating that less available energy went into ET, and more went into sensible heat flux (assuming similar amounts of net radiation, which was verified). On average, the increase in growing-season sensible heat flux is roughly 43 Wm^{-2}, which would be compensated for by a drop in ET of ~1.5 mm day^{-1} (i.e., roughly 180 mm over four months).

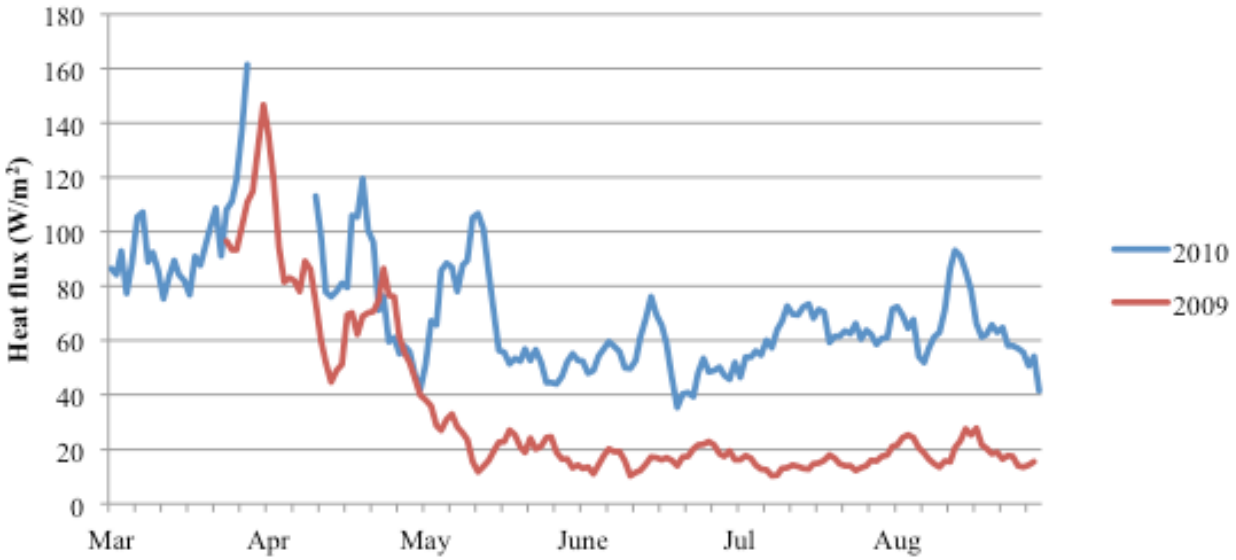

Figure 12. Five-day running mean LAS-derived sensible heat flux measurements from the *P. australis* wetland field site during 2009 (with live vegetation) and 2010 (with dead vegetation). Note the much higher sensible heat flux in 2010, starting around the beginning of the growing season (i.e., early May).

Measurements of soil temperature and water level / temperature were used to calculate the rate of heat storage in the wetland. We found that heat storage rates were much greater during the 2010 season as compared to the 2009 season. The total (i.e., cumulative) heat storage in the wetland during 2010 was roughly a factor-of-two higher than during 2009 (Figure 13), and we attribute this mainly to the reduced "insulating effect" of the dead vegetation (which also provides less shading of the underlying water and soil from solar radiation) and higher surface temperatures that resulted from the significant reduction in transpiration from standing vegetation.

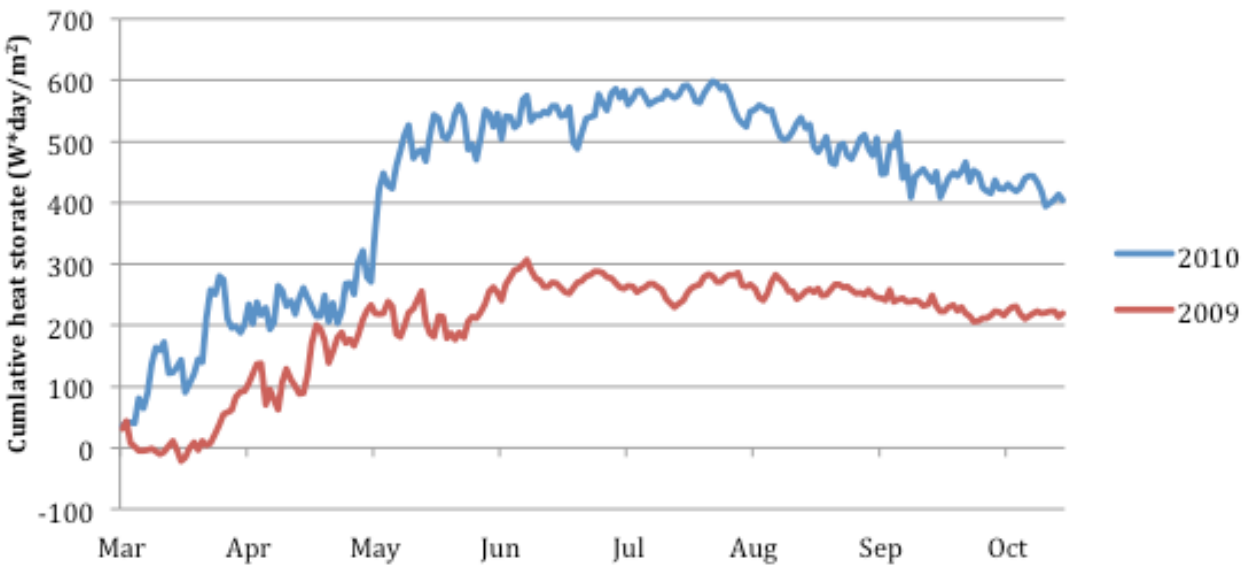

Figure 13. Total heat stored in the wetland (i.e., soil, water, and vegetation canopy) during 2009 and 2010 (accumulated through time starting at the beginning of each season).

A comparison of the ET rates for 2009 and 2010 are shown in Figure 14 (as latent heat flux, in W m^{-2}). It is clear that the spraying of the *P. australis* vegetation with herbicide had a significant impact on the wetland ET rate, reducing overall water consumption by roughly 32% (i.e., ~24 cm of water over the course of the growing season). Since the vegetation was not transpiring during 2010, the primary remaining source of ET in the wetland (Figure 14) was surface evaporation from standing water.

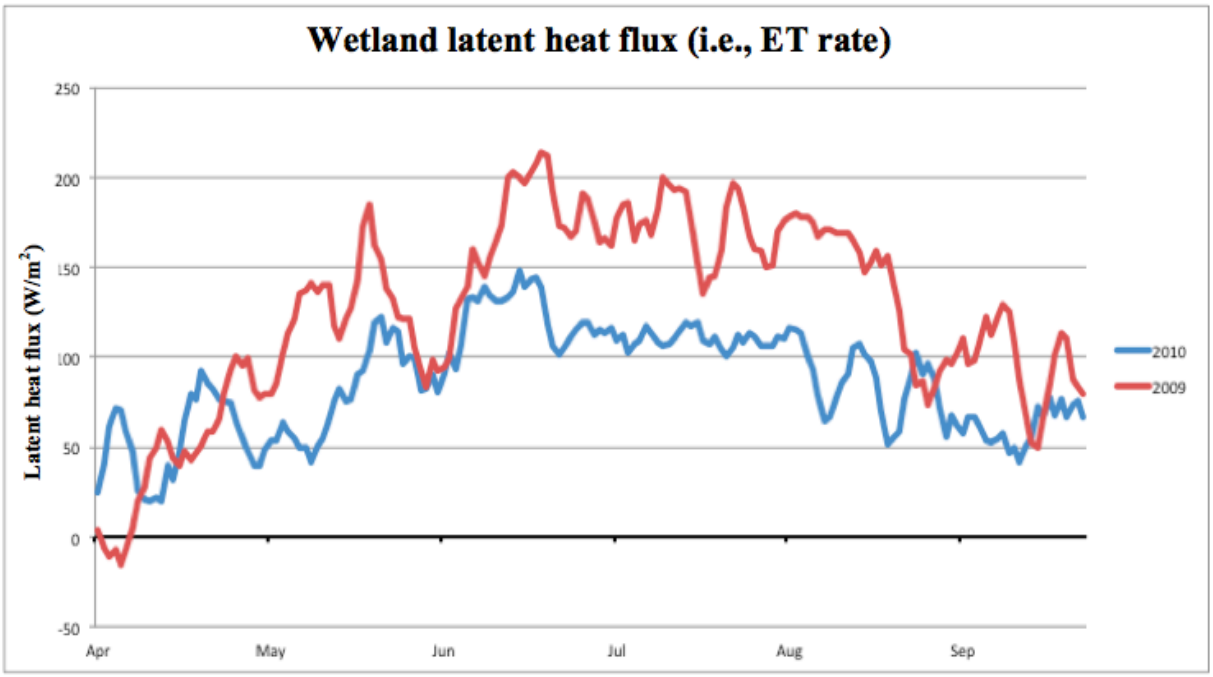

Figure 14. Latent heat flux measured at the *P. australis* wetland field site during the 2009 and 2010 growing seasons. A heat flux of 200 Wm^{-2} corresponds to roughly 7 mm day^{-1} of consumptive water use.

An additional example of the impact of vegetation removal on our wetland field site is shown in Figure 15, which displays a scatterplot of hourly mean surface water temperatures (in comparison to air temperatures) for 2009 and 2010. As would be expected, the general relationship shows warmer water temperatures during periods of warmer air temperature, with an overall scatter around the 1:1 line. However, a strong contrast is evident between the year with live *P. australis* vegetation (2009) and the year with dead vegetation (2010), especially during the main part of the growing season (June–August). In particular, it is clearly evident that – for the same air temperature – 2010 experienced significantly warmer water temperatures than 2009. On average, the increase in surface water temperature ranged from anywhere between 3°C to 7°C (Figure 15), which is a large change (e.g., well in excess of what might be anticipated to occur in response to short-term climate change). Given the similarity in other climatic variables between these two years (e.g., net radiation), this suggests a strong influence from the change in vegetation. More specifically, it indicates that the removal of *P. australis* can lead to significant warming of the underlying water and soil, which has important implications for not only surface evaporation rates, but also the surrounding wetland (or stream) ecosystem.

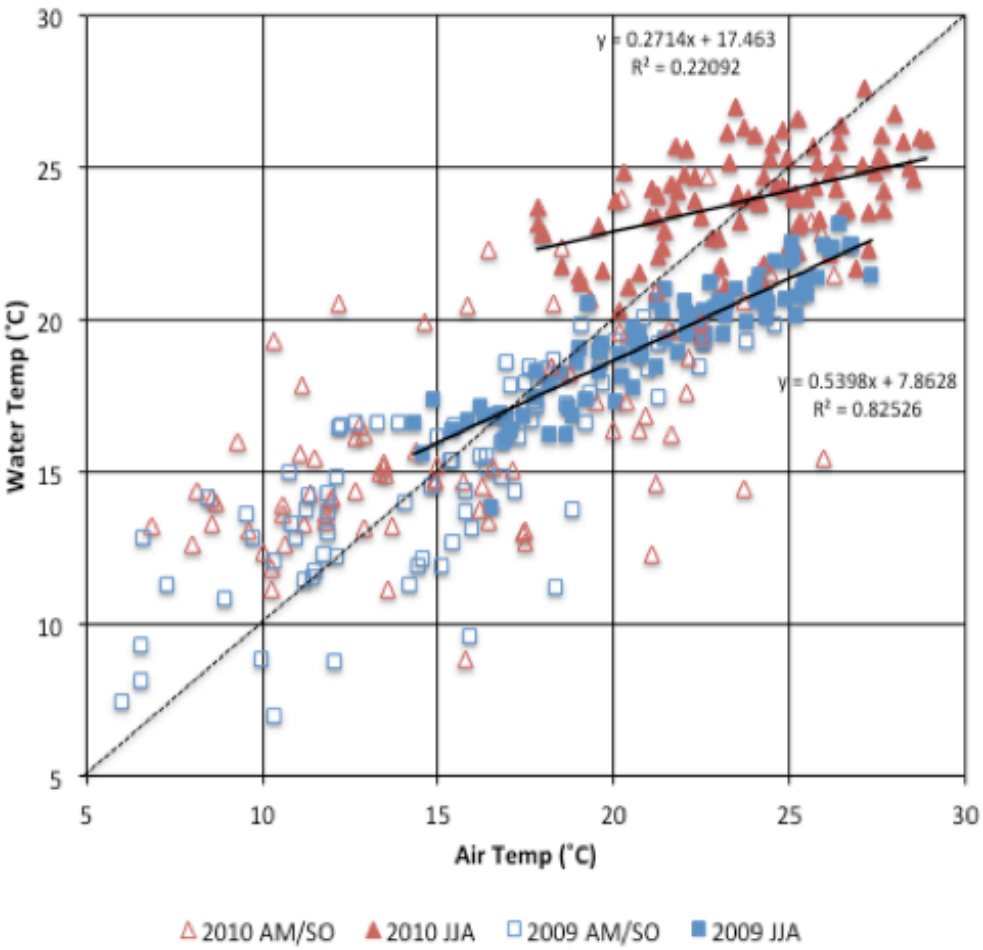

Figure 15. Scatterplot of observed, hourly mean surface water temperature vs. air temperature in the *P. australis* portion of the wetland during 2009 and 2010. The closed blue squares represent 2009 averages for the main growing season – June, July, and August (JJA) – while the open blue squares denote 2009 averages for April, May, September, and October (AM/SO). The red triangles represent similar values for 2010. Solid lines represent best-fit linear regressions, while the dashed line indicates the 1:1 line.

In general, the observational data has shown us that vegetation removal caused conditions at the wetland field site to be warmer, drier, and windier than in the presence of green *P. australis* (even after accounting for climatic differences between the two field seasons). These results are in agreement with conclusions from the energy balance analysis, which showed greater absorption of solar radiation, higher sensible heat flux, and significant reductions in ET at the wetland site. Reductions in ET are known to lead to lower ambient humidity, warmer surface temperatures, and – therefore – enhanced mixing of the atmospheric boundary layer. This latter effect is likely to be responsible for the observed increase in mean wind speed during 2010, which was much more dramatic in the *P. australis* portion of the wetland than in the section that was dominated by untreated native vegetation. This increase in wind speed is also consistent with the increase in sensible heat flux that was determined from the energy budget analysis.

4. Carbon dynamics, biogeochemistry and stream metabolism

Carbon dynamics in the P. australis wetland

During the growing season of 2009, carbon dynamics experiments were performed using soil and vegetation enclosures at the *P. australis* wetland field site. Soil respiration was found to be low relative to other components of the carbon balance, with significant differences between habitat types early in the season (Figure 16). Methanogenesis rates were roughly five times higher than soil respiration, with similar rates between all three habitat types (Figure 17). NEE_{Carbon} was highest in *P. australis* areas and displayed strong seasonality, peaking during late June (Figure 18). NEE of carbon also displayed strong diurnal variation, peaking in mid-afternoon, with *P. australis* showing the largest diurnal range (Figure 19).

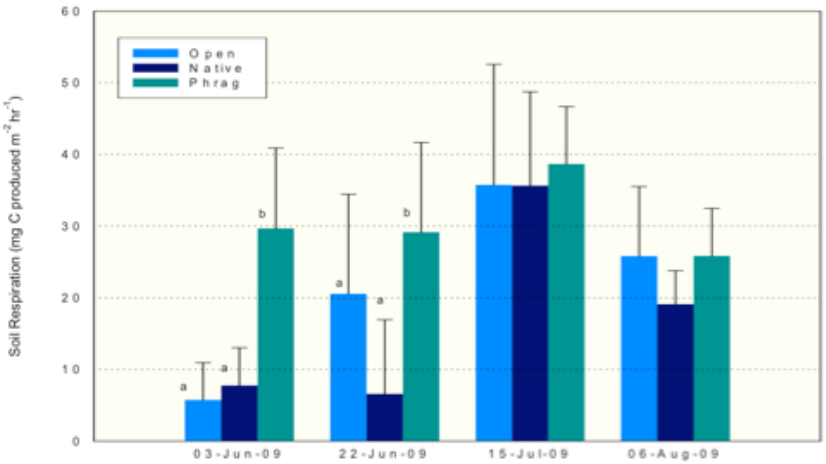

Figure 16. Soil respiration rates measured in PVC enclosures for three different habitat types over a 24-hour period. The bars labeled with different letters indicate that differences are statistically different at the 95% level ($\alpha = 0.05$).

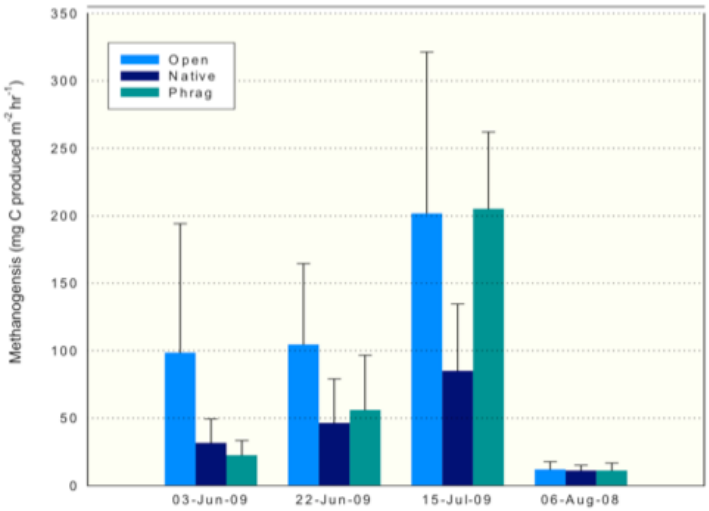

Figure 17. As in Figure 16, but for methanogenesis rates.

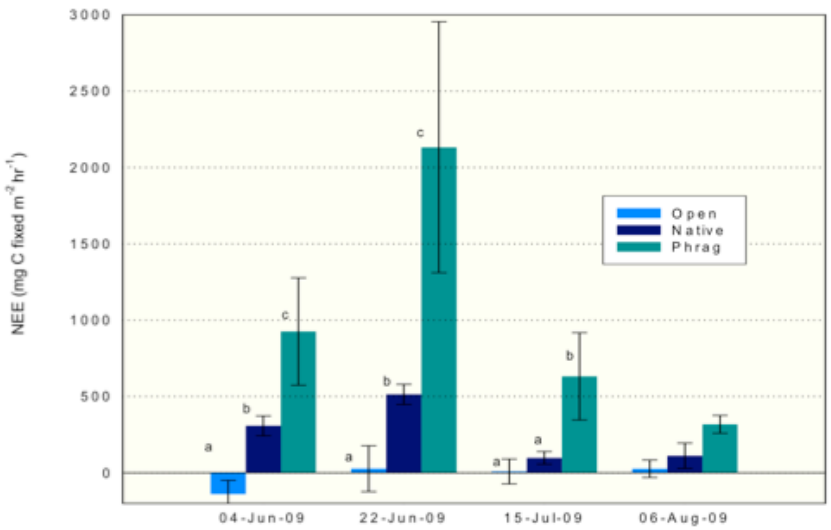

Figure 18. Seasonal variation of net ecosystem exchange of carbon for three different habitat types, measured with *in situ* carbon dioxide flux chambers.

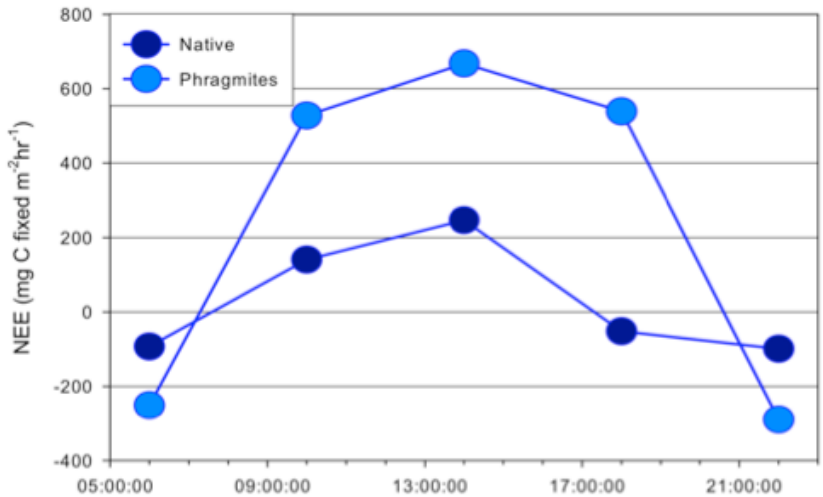

Figure 19. As in Figure 18, but for diurnal variation over a single 24-hour period (open-water habitat type is excluded).

Soil respiration rates were highest in the *P. australis* areas early in the season, but overall soil respiration does not appear to be a major source of carbon in this environment. On the other hand, methanogenesis was similar between all three habitat types and appears to be the major source of carbon compared to other studies conducted in natural wetlands. This has significant implications, as methane has a global warming potential that is 20 times higher than carbon dioxide. NEE_{Carbon} showed significant differences through the first three sampling dates, with *P. australis* fixing 2-5 times more carbon than open water and native areas during peak primary production periods. This finding was also supported by our data from the 24-hour run, which showed a higher nighttime carbon flux in *P. australis* but (over a daily period) a much higher potential to fix carbon compared to native species and open water areas.

Impact of P. australis on wetland biogeochemistry

Biogeochemical data from the sediments of three riverine wetlands in Nebraska were collected in fall 2008, spring 2009, and summer 2009. Sites included in this study range from heavily (Arapahoe) to moderately (Martin's Reach) to sparsely (Bassway Pond) infested with *P. australis.* The data suggest that the impact of *P. australis* on carbon and nitrogen cycling in soils was greatest in the heavily infested site and that these cycles were enhanced in soils beneath invasive species compared to native species. Specifically, we observed higher organic matter concentrations underneath *P. australis* (Figure 20) despite labile carbon rates also being high in the Arapahoe site (Figure 21). This is most likely a result of the prolific aboveground biomass produced by *P. australis* compared to much smaller native species such as sedges and rush. Further, the higher labile carbon pool supports greater concentrations of microbial biomass (Figure 22) and this, in turn, fuels higher rates of nitrogen cycling (Figures 23 and 24).

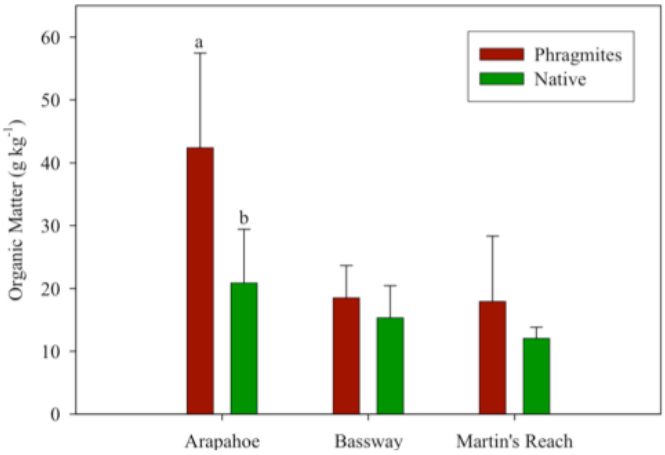

Figure 20. Soil organic matter concentrations observed at the three study sites beneath *P. australis* and native species (either sedge or rush). The results indicate that sediments beneath *P. australis* accumulate more carbon, particularly at the heavily infested site (Arapahoe).

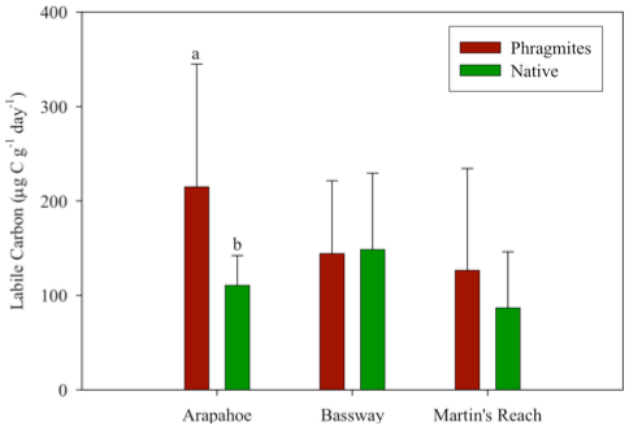

Figure 21. Labile carbon rates obtained from sediments collected at the three study sites. At the heavily infested site (Arapahoe), sediments beneath *P. australis* have greater rates of easily degradable carbon, suggesting that these sediments can support more abundant microbial communities.

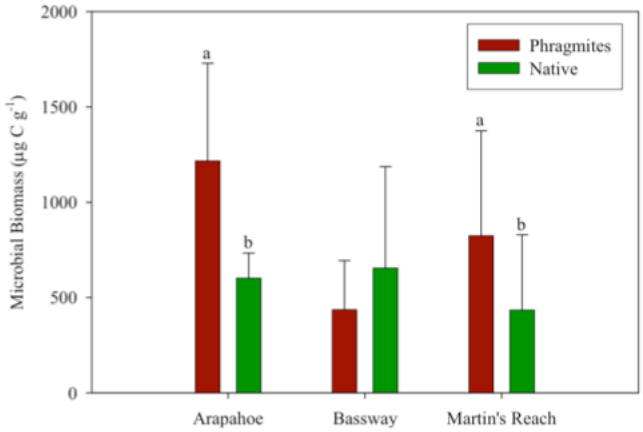

Figure 22. Estimates of microbial biomass in sediments collected at the three study sites. In the two most infested sites, the microbial communities are most abundant beneath *P. australis* compared to native species.

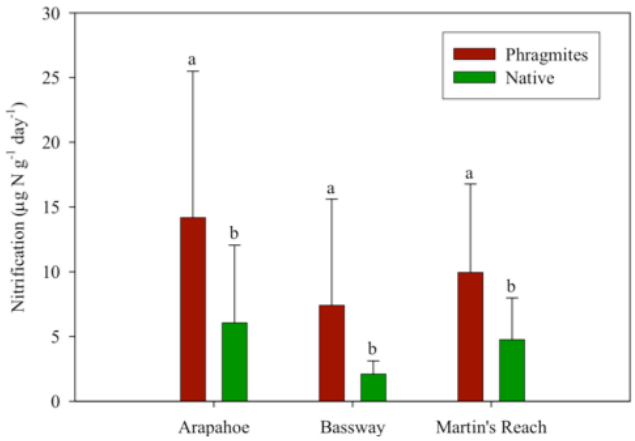

Figure 23. Nitrification rates observed at the three study sites. (Nitrification is a process that converts ammonia – a compound that is toxic to aquatic biota – to nitrate.) Results show that rates are higher beneath *P. australis* at all sites.

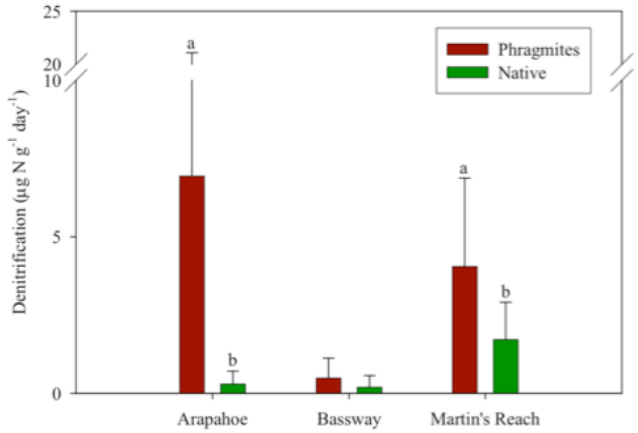

Figure 24. Denitrification rates observed at the three study sites. (Denitrification is a process that removes nitrate from an ecosystem by converting it to nitrogen gas.) Results show that rates are higher beneath *P. australis* at the two most infested sites.

In summary, this project has found that the infestation of a wetland with *P. australis* results in more carbon sequestration and a greater microbial abundance, which can cycle and remove nitrogen at higher rates. This is most likely due to the trapping of fine sediments in dense stands of *P. australis.* The fine materials contain more labile carbon, which is bio-available to microbes, and higher surface area for microbes to colonize. Thus, the infestation of *P. australis* in riverine wetlands in Nebraska is enhancing biogeochemical processes, but at the same time is irreparably altering sediment structure.

Effects on stream metabolism

During the fall of 2009, monitoring stations were set up along the South Channel of the Platte River to measure water chemistry and stream metabolism (Figure 25). Stream metabolism is a method for measuring the overall change in the primary productivity and respiration (two biological mechanisms responsible for changing dissolved oxygen) in a stream ecosystem. The objective of this portion of the study was to measure the impacts of herbicide treatment of *P. australis* on a stream ecosystem. Preliminary data from a controlled greenhouse experiment revealed that herbicide treatment of riparian vegetation could result in ammonium export to nearby streams and rivers. If ammonium export was significant, this could lead to a fertilizing effect on the stream and allow for excessive algal growth. Excessive algal growth would then create shifts in dissolved oxygen levels and harm aquatic organisms (i.e., eutrophication).

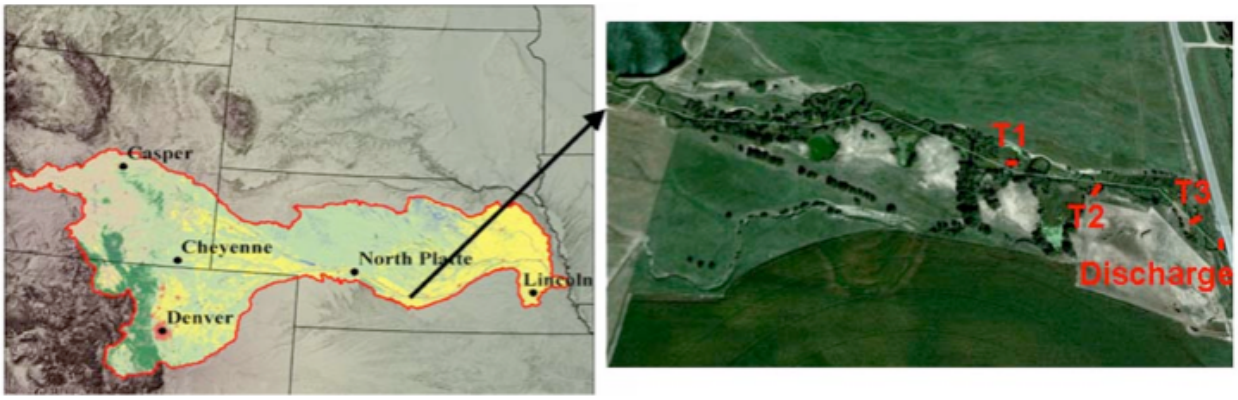

Figure 25. Left: Location of the Platte River Basin and of our study stream. Right: Aerial image of the South Channel of the Platte River and the three study transects and discharge transect.

At each transect, ISCO samplers were installed to collect water samples for chemical analysis, and YSI multi-parameter sondes were installed to measure stream temperature, specific conductance, and dissolved oxygen. We also established a discharge transect and installed an In Situ Level TROLL pressure transducer to measure continuous discharge at the site. Two sampling efforts were coordinated to monitor the stream prior to herbicide treatment (September 18-21) and to monitor the stream during the herbicide treatment that occurred at 13:15 on September 25, 2009 and shortly thereafter (September 24-27).

Approximately 50 meters downstream of the last transect, a well equipped with an In Situ Level TROLL pressure transducer was installed, and a discharge transect was established. On six occasions stream discharge was measured in the field using the six-tenths depth method and a Marsh McBirney Flow Mate velocity meter. Discharge was regressed against the barometrically corrected pressure reading to develop a stage-discharge relationship. From this relationship a continuous record of discharge was derived for the stream site (Figure 26).

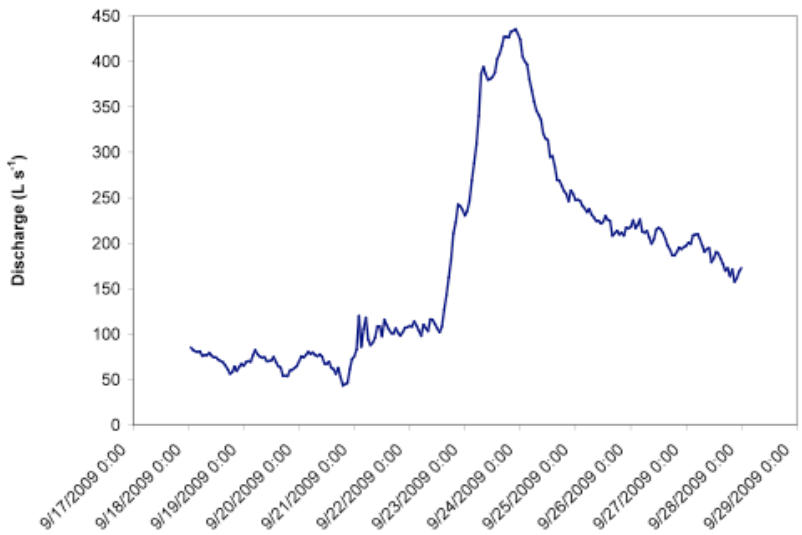

Figure 26. Continuous discharge record for the South Channel of the Platte River during the study period.

To measure stream metabolism, we used the open channel method developed by Odum (1956) that examines the change in oxygen over a diurnal period. Three factors can influence dissolved oxygen in a stream: 1) Temperature, 2) primary production or respiration from algae or bacteria, and 3) interaction with atmospheric oxygen (reaeration). This method factors out the change in oxygen due to temperature, measures the reaeration rate, and thus estimates stream metabolism (i.e., the change in oxygen due to primary production and/or respiration).

Using dissolved oxygen data from all three transects along the stream we calculated primary productivity and respiration for the stream during a three-day period (September 18-21) prior to herbicide treatment (Figure 27). Overall, during this pre-treatment monitoring, both primary production and respiration were high but not excessive (values ranged from 6-13 g O_2 m^{-2} d^{-1}). Herbicide treatment of the riparian *P. australis* took place at 13:15 on September 25, 2009 and was applied at all three transects. Data from September 24 indicate that primary production and respiration were still high (values ranged from 6-16 g O_2 m^{-2} d^{-1}) but within the range of the pre-treatment values. Treatment occurred late enough in the day on September 25 to not affect stream metabolism. However, during the following day, both primary production and respiration significantly increased (values ranged from 22-32 g O_2 m^{-2} d^{-1}). Water chemistry data from the stream revealed that the largest increase in ammonium load was due to the flood event on September 23 (Figure 28). However, ammonium loads also increased late in the day on September 25 and early September 26. Results from our greenhouse experiment suggest that this increase was due to the isopropylamine salt present in the herbicide (as a surfactant).

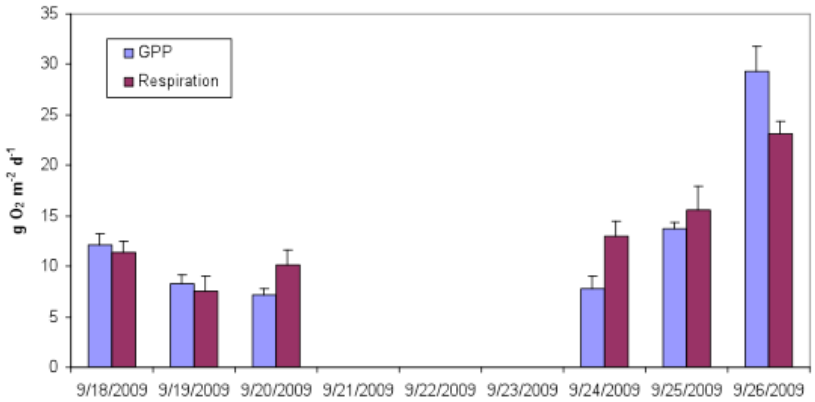

Figure 27. Gross primary production (GPP) and respiration values for all three transects during the pre-treatment period (September 18-21) and the post-treatment period (September 24-26). Herbicides were applied via a helicopter at 13:15 on September 25, 2009 at all three transects.

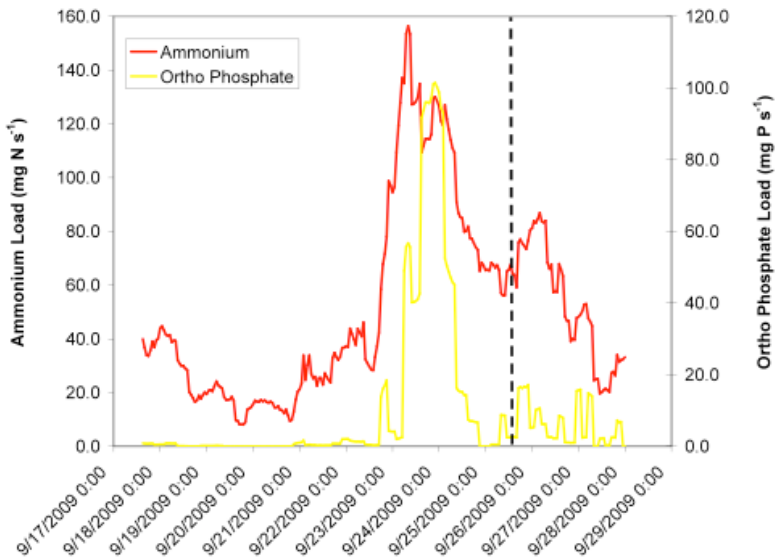

Figure 28. Water chemistry data showing the ammonium load (mg N s^{-1}) and orthophosphate load (mg P s^{-1}) during the study. The peak during September 23-24 is due to a flood pulse moving through the system. The dashed line represents the time at which the helicopter treated the stream with herbicide.

This study suggests that herbicide treatment of riparian vegetation has a pronounced impact on stream metabolism. In particular, herbicide treatment creates a "fertilizing effect" on the stream and causes both primary production and respiration to increase significantly. If the treated stream has low nutrient loads prior to herbicide treatment and is a relatively pristine system, then the "fertilizing effect" could have detrimental impacts on aquatic biota. In particular, nighttime dissolved oxygen levels could drop to low concentrations and cause fish kills. The South Channel of the Platte River, on the other hand, had high nutrient levels prior to treatment and is a moderately polluted stream due to nearby agricultural land use. Therefore, our study stream had some buffering capacity, and nighttime dissolved oxygen levels never dropped below 6 mg L^{-1}. (Aquatic biota become stressed when dissolved oxygen levels drop below 4 mg L^{-1}.)

5. Growth Chamber Measurements of Plant Physiology

Growth chamber experiments, which were initiated during the 2011 growing season, were used to measure physiological parameters necessary for simulating *P. australis* in the Agro-IBIS model. Experiments were performed on both invasive and native *P. australis* samples collected from our field site and from north of Grand Island, respectively, as well as fertilized versus non-fertilized varieties. Parameters such as photosynthetic rate (A), dark respiration (R_d), transpiration (E), and stomatal conductance (g_s) were all measured directly by a LI-COR 6400 gas exchange analyzer (Figure 29). Additional parameters such as maximum carboxylation velocity (V_{max}), maximum electron transport (J_{max}), chlorophyll fluoresence (F_v/F_m), and quantum efficiency (Φ) were calculated through non-linear regressions using SAS (Figure 30). Specific leaf area measurements and isotope analysis (N and C) were also performed for the *P. australis* leaf samples.

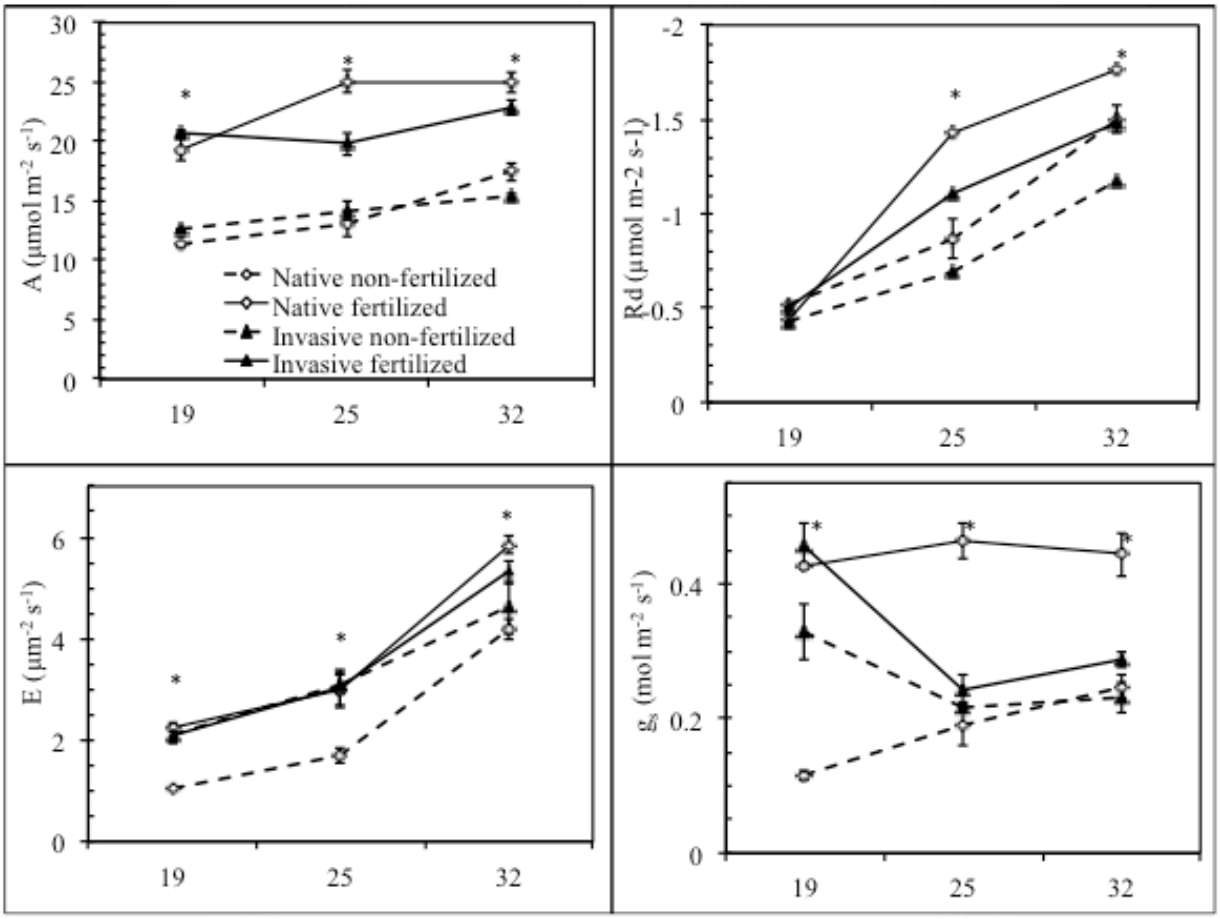

Figure 29. Measured plant physiological parameters from the *P. australis* growth chamber study.

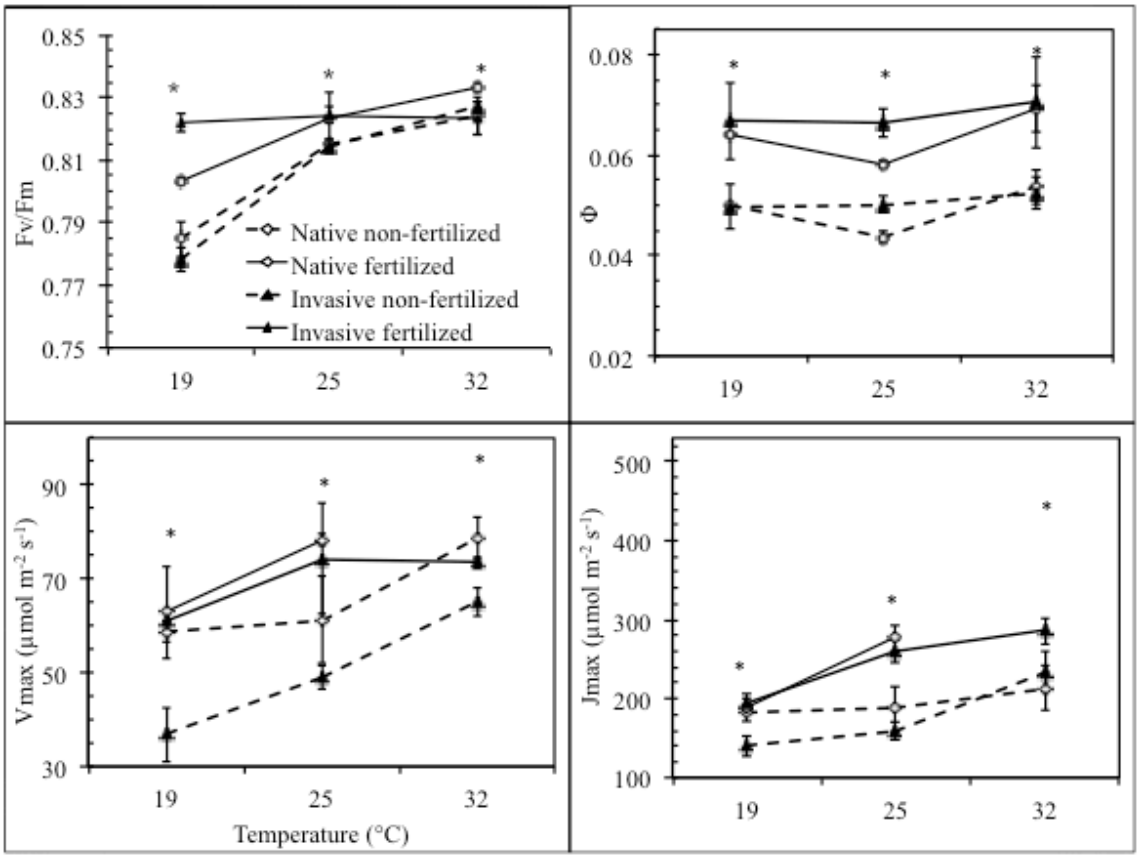

Figure 30. Calculated parameters from the *P. australis* growth chamber study. (V_{max} and J_{max} values for the native-fertilized subset were unrealistically high at 32℃ and were removed from the analysis.)

Except for stomatal conductance (g_s), all measured parameters in Figure 29 generally show higher values at higher ambient temperatures. Fertilization of both varieties of *P. australis* had a positive effect on each parameter, with higher values than each non-fertilized variety. In the fertilized experiments, the native subset outperformed the invasive subset for every measured parameter, while for the non-fertilized scenarios, the invasive subset generally outperformed the native subset (though not as drastically; Figure 29). As with the measured variables, all calculated parameters showed a general positive trend with increasing temperature and increased fertilization (Figure 30).

In addition, isotopic analyses of samples were collected as part of these experiments. Figure 31 shows some of the results of this analysis for the four sets of *P. australis* plants that were grown in the growth chamber. The scatterplot in Figure 31 displays the carbon isotope ratio ($C^{13}\delta$) as a function of water use efficiency (WUE). From this figure, it is evident that fertilization had a positive impact on WUE and also caused a slight increase in the ratio of $C^{13}\delta$. The native *P. australis* also had much higher water use efficiencies and slightly higher $C^{13}\delta$ values than the invasive variety. Lower WUE and $C^{13}\delta$ values are often indicative of invasive species, and the invasive variety of *P. australis* displayed these same characteristics in our study. Plants better adapted to hot and arid environments typically display higher WUE and $C^{13}\delta$ values than other plants, suggesting that native *P. australis* may be better suited for warmer, drier regions of Nebraska than the invasive variety.

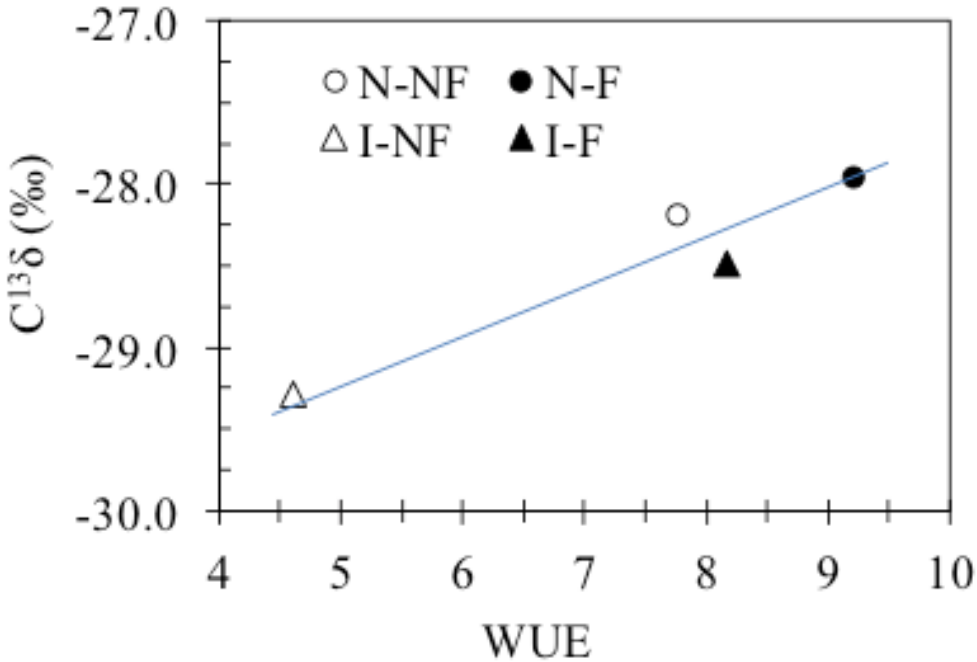

Figure 31. Carbon isotope ratio ($C^{13}\delta$) as a function of water use efficiency (WUE) for fertilized (F) and non-fertilized (NF) native (N) and invasive (I) *P. australis* under growth chamber conditions.

The above physiological parameters for *P. australis* were incorporated into the Agro-IBIS model and resulted in a 15% improvement in the simulated ET for *P. australis* (as compared to observations at our wetland field site and to results from previous Agro-IBIS simulations). These model results are discussed in the next section.

6. Agro-IBIS model results

Agro-IBIS simulations at the wetland field site

To simulate the water and energy balance in the *P. australis*-dominated wetland, a number of changes were made to the Agro-IBIS source code. These changes include adjustments to plant physiological parameters based on our field observations, as well as modifications to the soil water flux algorithm to incorporate a groundwater component and simulate wetland conditions properly. Some modifications related to plant physiology are explained below.

A version of Agro-IBIS that had been developed for energy crops (switchgrass and *Miscanthus giganteus)* was modified to accurately simulate *P. australis* using physiological parameters that were measured in the greenhouse experiments and in the field. Adjusted parameters included initial leaf area index (LAI), maximum LAI, plant height, specific leaf area, and V_{max}. Other model inputs such as the rate of LAI decline and the number of growing degree days (GDD) required for leaf emergence, plant browning, and plant maturity were also adjusted to better

match observed latent heat flux values for *P. australis* (measured at our field site in 2009). The resulting graph of evapotranspiration (ET) rates (Figure 32) shows a strong correspondence with observed data from the wetland field site (r = 0.96, RMSE = 18.8 Wm^{-2}) and a 15% reduction in error compared to previous model runs (r = 0.92, RMSE = 22.1 Wm^{-2}), which had simply approximated *P. australis* by using "corn" as the vegetation type. This improvement in modeled ET is especially noticeable early in the season.

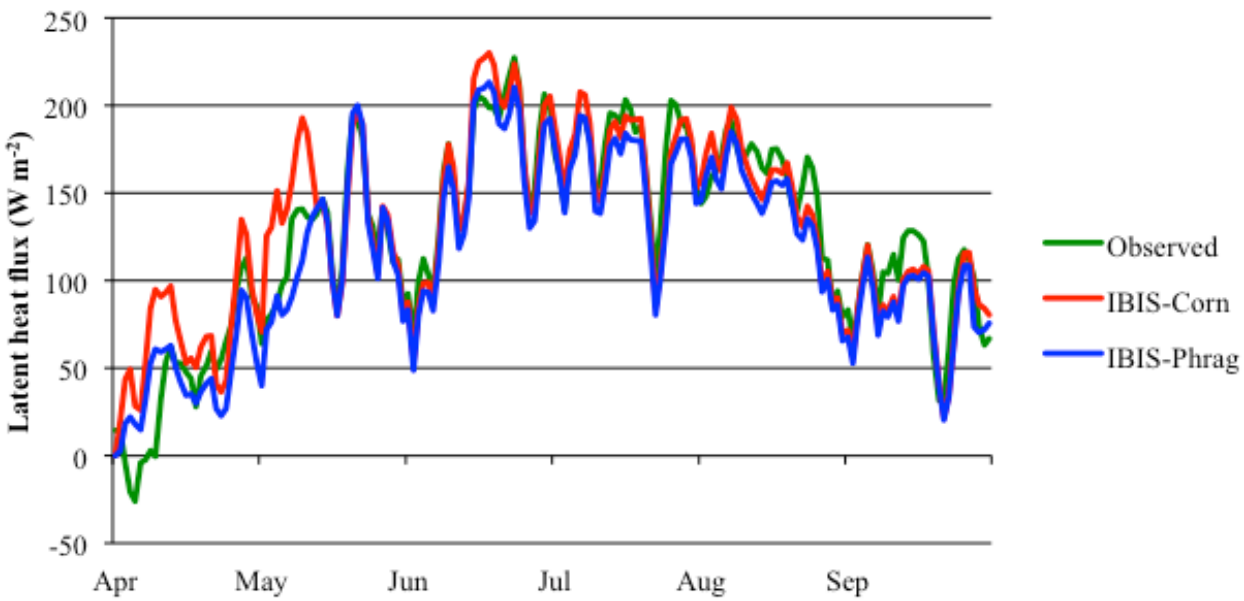

Figure 32. Observed (green) and modeled (red and blue) latent heat flux (i.e., evapotranspiration rate) for the 2009 growing season using corn (red) and *P. australis* (blue) as the modeled vegetation types in Agro-IBIS.

Agro-IBIS regional simulations

Agro-IBIS was used to analyze the impact of interannual climate variability on summer ET rates for both "natural" vegetation (grassland and savanna) and invasive *P. australis* across the state of Nebraska and surrounding regions (including the Republican River basin). This is our first "broad-scale" application of a high-resolution version of the Agro-IBIS model to understanding the relative roles of climate and vegetation across the Republican River basin. The model simulations include a scenario in which the entire region is covered with *P. australis* to test the hypothetical response to full infestation by the invasive species. To examine changes in ET in response to interannual variations in climate for both vegetation types, we applied two climate scenarios by increasing and decreasing the summer mean precipitation by a factor of 1.5, together with co-varying changes in solar radiation, relative humidity, and daily maximum and minimum air temperatures. The co-varying scenarios were determined from observed, historical climate variability in the region. Table 2 shows the changes in each climatic parameter, in association with the prescribed changes in precipitation.

Table 2. Two interannual climate scenarios utilized in the Agro-IBIS model simulations in association with factor-of-1.5 increases and decreases in precipitation, *P* (wet and dry scenarios respectively). Co-varying changes in incoming shortwave radiation (*SW*), maximum and minimum daily temperature (T_{max} and T_{min}), and relative humidity (*RH*) were determined from observed, interannual climate variability in the region (throughout the state of Nebraska and surrounding regions). The delta symbol (Δ) refers to changes in each parameter.

ΔP (%)	ΔSW (%)	ΔT_{max} (°C)	ΔT_{min} (°C)	ΔRH (%)
+50.0	-12.4	-2.6	-1.6	+16.0
-33.0	+5.3	+2.3	+1.1	-9.9

Agro-IBIS was run at 5-minute spatial resolution (~8 km), with an hourly time step and a spin-up period of 10 years, which allowed the model to reach equilibrium. We selected the summer of 1990 (June, July, and August) as our "control year" for both simulation scenarios, because this year shows relatively small climatic anomalies and is also not preceded by a series of anomalous years. Climatic perturbations were then applied to this control simulation using the two scenarios outlined in Table 2. The "natural vegetation" dataset was derived from the International Geosphere Biosphere Programme's 1-km DISCover land cover dataset, while the *P. australis* simulations were achieved by implementing "modified corn" as the plant functional type, which we previously found to be the most suitable means of representing *P. australis* in Agro-IBIS (as determined in simulations validated at our wetland field site).

The results of the Agro-IBIS control simulation are shown in Figure 33. As is well known, there is a well-defined radiation and moisture gradient across the state of Nebraska and surrounding regions (Figures 33a and 33b). The large precipitation gradient leads to a similarly large east-west gradient in simulated ET in both simulations (Figures 33c and 33d), with highest ET rates occurring in the eastern parts of the region. One might expect *P. australis* to show higher rates of ET than natural vegetation, and this is found to be true over the eastern domain. Interestingly, however, this is not the case in the drier, western domain, where natural vegetation shows slightly higher rates of ET. It is important to note, however, that these simulations do not include any influence from shallow groundwater (i.e., the default "free drainage" is allowed to occur at the bottom of the modeled soil profile).

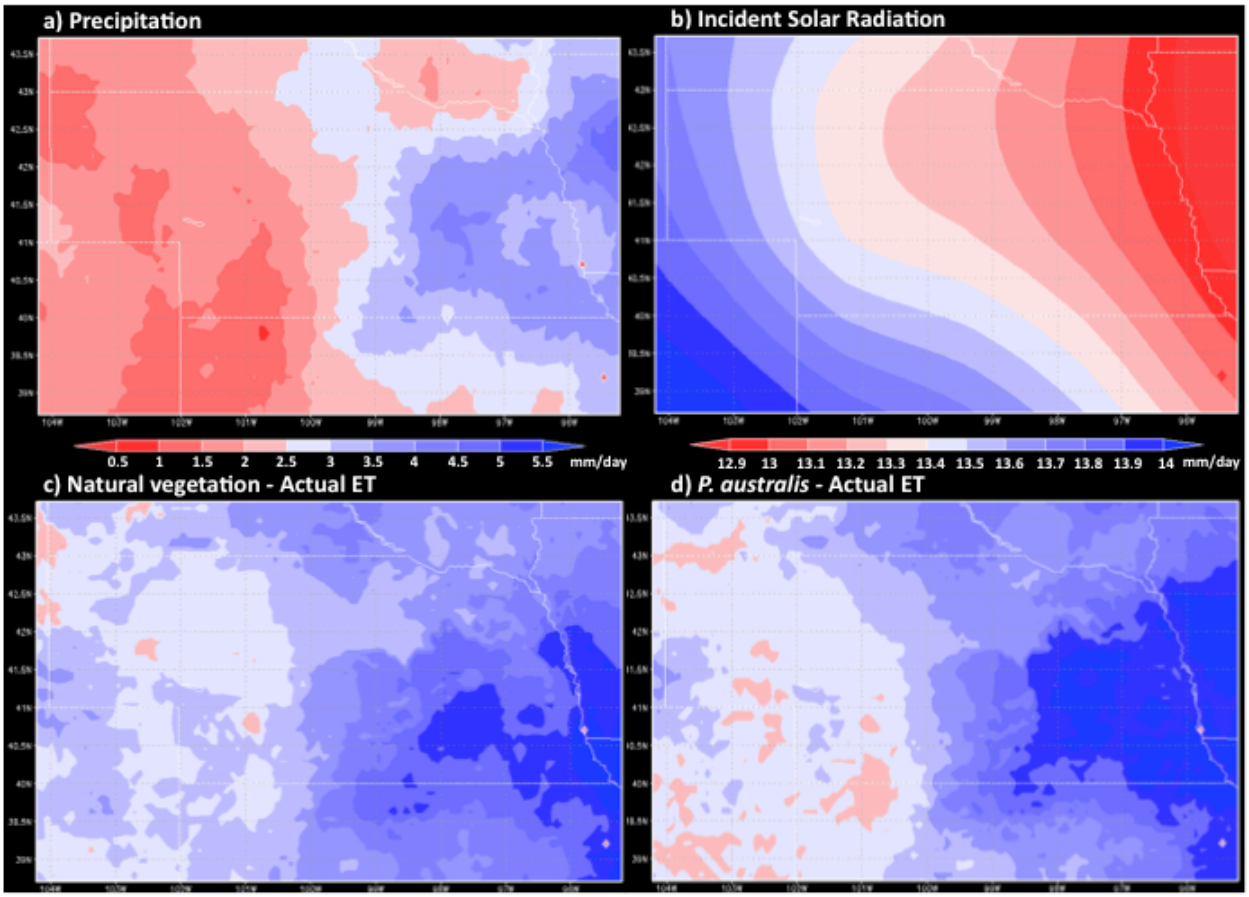

Figure 33. Climatic input and output parameters in the Agro-IBIS model simulations, including a) precipitation, b) incoming solar radiation, and simulated ET for c) *P. australis* and d) natural vegetation during the 1990 summer period (June–August). All units are mm/day (with solar radiation converted to an equivalent rate of ET, or latent heat flux).

The model-simulated changes in ET due to interannual changes in climate (as defined in Table 2) are shown in Figure 34. In general, it is found that increases in precipitation lead to increases in ET in the western domain due to greater water availability but decreases in ET in the eastern domain due to increases in cloud cover and associated reductions in available energy. Decreases in precipitation, on the other hand, lead to reductions in ET throughout the entire domain (Figures 34b and 34d). The ET response is generally found to be stronger in the case of the *P. australis* vegetation (Figures 34a and 34b), as opposed to the natural vegetation scenarios (Figures 34c and 34d). For example, a 50% increase in precipitation leads to about a 15-50% increase in ET in the western domain for the *P. australis* scenario, but only a 5-20% increase for natural vegetation. This reflects the relatively high consumptive water use of *P. australis* vegetation, particularly during wet conditions. Note that this also implies (for *P. australis,* in comparison to natural vegetation) a weaker increase in runoff during wet summers.

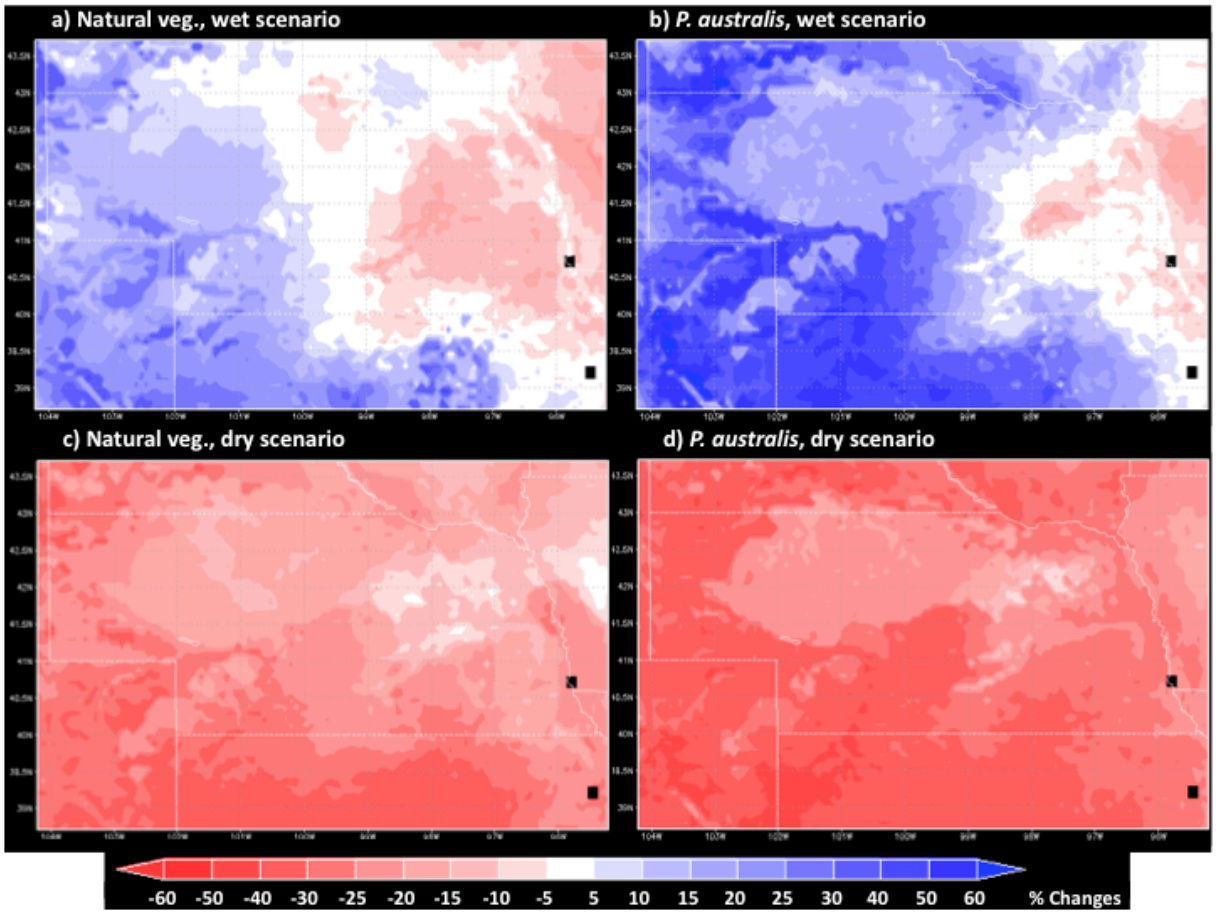

Figure 34. Agro-IBIS model-simulated changes in ET in response to wet and dry scenarios (as listed in Table 2). Shown are the percent changes in ET from the control simulations using *P. australis* and natural vegetation. a) and b) show percent ET deviation of *P. australis* for increased and decreased precipitation scenarios, respectively, while c) and d) show percent ET deviation of natural land cover for increased and decreased precipitation scenarios, respectively, from control runs.

7. List of publications

Cutrell, G. J. (2010) Seasonal Energy and Water Balance of a *Phragmites Australis*-Dominated Wetland in the Republican River Basin (Southwestern Nebraska, USA). M.S. Thesis. University of Nebraska-Lincoln. 128 pp.

Herrman, KS, DT Scott, J.D. Lenters, and E. Instanbulluoglu, (2012). Nutrient loss following *Phragmites australis* removal in controlled soil mesocosms. *Water, Air & Soil Pollution, 223, 1-12.*

Istanbulluoglu E., T. Wang, O. M. Wright, and J.D. Lenters (2012). Interpretation of Hydrological Trends from a water balance perspective: The role of groundwater storage in the Budyko hypothesis, Water Resour. Res., 48, W00H16, doi:10.1029/ 2010WR010100.

Lenters, J.D., Cutrell, G.T., Istanbulluoglu, E., Scott, D.T., Herrman, K.S., Irmak, A., Eisenhauer, D.E., (2011). Seasonal energy and water balance of a*Phragmites australis*-dominated wetland in the Republican River basin of south-central Nebraska (USA). *Journal of Hydrology, 408*, 19-34.

Soylu, M.E. (2011). Quantifying evapotranspiration and water table interactions in regions of shallow groundwater: sensitivity to soil properties, vegetation, and climate variability. Ph.D. dissertation, University of Nebraska – Lincoln, 208 p

Soylu, M. E., Istanbulluoglu, E., Lenters, J. D., and Wang, T., (2011). Quantifying the impact of groundwater depth on evapotranspiration in a semi -arid grassland region. *Hydrol. Earth Syst. Sci.*, **15**, 787–806, http://www.hydrol-earth-syst-sci.net/15/787/2011/hess-15-787-2011.html, doi:10.5194/hess-15-787-2011.

Soylu, M.E., Lenters, J.D., Istanbulluoglu, E., Loheide II, S.P: On evapotranspiration and shallow groundwater fluctuations: A Fourier-based improvement to the White method, *Water Resources Research* (in press).

Wang, T., E. Istanbulluoglu, J. D. Lenters, and D.T. Scott (2009). On the role of groundwater and soil texture in the regional water balance: An Investigation in the Nebraska Sand Hills, USA. Water Resour. Res., 45, W10413, doi:10.1029/2009WR007733.

Walters, S. (2010). Carbon dynamics in a *Phragmites australis* invaded riparian wetland. M.S. Thesis. University of Nebraska-Lincoln. 53 pp.

8. List of presentations

Cutrell, G. J. Analysis of the Energy and Water Balance of a Temperate Wetland and the Response to Changes in Climate and Vegetation. Division of Natural Resources Brown Bag Seminar, Oral Presentation, Nebraska State Office building, 2009, Lincoln NE.

Cutrell, G., Lenters, J, Herrman, K, Istanbulluoglu, E, Scott, D, Soylu, M.E, Walters, S, Wang, T. Analysis of the Energy and Water Balance of a Temperate Wetland and the Response to Changes in Climate and Vegetation. American Meteorological Socity, 2010 Annual Meeting, Poster Presentation, Atlanta, GA.

Mykleby, P.M., Lenters, J.D., Cutrell, G.T., Herrman, K.S., Istanbulluoglu, E., Scott, D.T.: Water and Energy Balance Response in Response to the Removal of Invasive Phragmites australis in a Riparian Wetland, UNL Water Center, Water Law Conference and Great Plains Climate and Ecosystems 2011, poster presentation 2011, Lincoln, NE.

Mykleby, P.M., Lenters, J.D., Cutrell, G.T., Herrman, K.S., Istanbulluoglu, E., Scott, D.T.: Water and Energy Balance Response in Response to the Removal of Invasive Phragmites australis in a Riparian Wetland, American Geophysical Union, Fall 2011, poster presentation, abstract #H33D-1343, San Francisco, CA.

Soylu, M.E., Lenters, J.D., Istanbulluoglu, E.: On evapotranspiration and shallow groundwater fluctuations: A Fourier-based improvement to the White method and the role of specific yield under saturated conditions, American Geophysical Union, Fall Meeting 2011, oral presentation, San Franciso, CA.

Soylu, M.E., Lenters, J.D., Dong, B., Sensitivity of evapotranspiration to variations in climate and land cover in the Central Great Plains, UNL Water Center, Water Law Conference and Great Plains Climate and Ecosystems 2011, poster presentation, 2011, Lincoln, NE.

Soylu, M. E., Wang, T., Istanbulluoglu, E., Lenters, J. D.: Quantifying the impact of groundwater depth on evapotranspiration in a semi arid grassland region, American Geophysical Union, Fall Meeting 2009, poster presentation, abstract #H41C-0903, San Franciso, CA.